Biochimica et Biophysica Acta 1837 (2014) 1553–1566

Contents lists available at ScienceDirect

Biochimica et Biophysica Acta

journal homepage: www.elsevier.com/locate/bbabio

Review

Growing green electricity: Progress and strategies for use of Photosystem I for sustainable photovoltaic energy conversion ☆

Khoa Nguyen [a], Barry D. Bruce [a,b,c,*]

[a] Department of Biochemistry and Cellular and Molecular Biology, University of Tennessee, Knoxville, TN 37996, USA
[b] Department of Microbiology, University of Tennessee, Knoxville, TN 37996, USA
[c] Bredesen Center for Interdisciplinary Research and Education, University of Tennessee, Knoxville, TN 37996, USA

ARTICLE INFO

Article history:
Received 22 November 2013
Received in revised form 17 December 2013
Accepted 25 December 2013
Available online 3 January 2014

Keywords:
Photosystem I
Photocurrent
Photovoltaic
Biohybrid

ABSTRACT

Oxygenic photosynthesis is driven via sequential action of Photosystem II (PSII) and (PSI)reaction centers via the Z-scheme. Both of these pigment–membrane protein complexes are found in cyanobacteria, algae, and plants. Unlike PSII, PSI is remarkably stable and does not undergo limiting photo-damage. This stability, as well as other fundamental structural differences, makes PSI the most attractive reaction centers for applied photosynthetic applications. These applied applications exploit the efficient light harvesting and high quantum yield of PSI where the isolated PSI particles are redeployed providing electrons directly as a photocurrent or, via a coupled catalyst to yield H_2. Recent advances in molecular genetics, synthetic biology, and nanotechnology have merged to allow PSI to be integrated into a myriad of biohybrid devices. In photocurrent producing devices, PSI has been immobilized onto various electrode substrates with a continuously evolving toolkit of strategies and novel reagents. However, these innovative yet highly variable designs make it difficult to identify the rate-limiting steps and/or components that function as bottlenecks in PSI-biohybrid devices. In this study we aim to highlight these recent advances with a focus on identifying the similarities and differences in electrode surfaces, immobilization/orientation strategies, and artificial redox mediators. Collectively this work has been able to maintain an annual increase in photocurrent density (A cm^{-2}) of ~10-fold over the past decade. The potential drawbacks and attractive features of some of these schemes are also discussed with their feasibility on a large-scale. As an environmentally benign and renewable resource, PSI may provide a new sustainable source of bioenergy. This article is part of a Special Issue entitled: Photosynthesis Research for Sustainability: Keys to Produce Clean Energy.

1. Introduction

Photosynthetic reaction centers are chlorophyll (Chl) pigment–protein complexes capable of converting light energy into a stable charge separation. In oxygenic photosynthesis, Photosystem II (PSII) and Photosystem I (PSI) work in series to couple the splitting of water with the reduction of ferredoxin [1]. Whereas PSII has evolved to have a strong oxidizing potential, PSI has evolved to have a low potential acceptor that is capable of reducing $NADP^+$ via the soluble Fe/S protein ferredoxin and the flavin protein FNR. In plants, some algae, and some cyanobacteria, the electron donor to photo-oxidized PSI (P_{700}^+) is plastocyanin, while in other cyanobacteria and algae a soluble c-type cytochrome (cyt c_6 or cyt c_{553}) serves as the donor [2]. There are many excellent reviews that cover the kinetics and thermodynamics of electron transfer of PSI [3–9], which are shown in Fig. 1.

Considerable interest has recently been directed to the utilization of its charge separation with applied goals in solar energy applications such as hydrogen production [10,11] and generation of photocurrent in photovoltaic devices [12,13], exploiting the robust and highly efficient nature of PSI [14]. There have also been similar advances in the use of PSI for light driven hydrogen production and are addressed in other recent papers [11,15,16]. In this review we cover many of the recent advances in the utilization of PSI for photovoltaic purposes.

2. Powers and versatility of PSI reaction centers

PSI is an example of a Type I reaction center which has a different acceptor system than Type II reaction centers [17]. For example, Type I reaction centers, in contrast to the dual quinone acceptors, Q_A and Q_B, in the Type II reaction centers of purple bacteria and Photosystem II, have an FeS center that functions as the first stable acceptor (shown as F_X in Fig. 1). This is similar to the reaction centers found in the green sulfur bacteria [18] and the heliobacteria [19]. Another feature of the Type I reaction center is that the special pair, P_{700} produces a much stronger electron donor when excited and P_{700}^* has a midpoint potential of −1.3 V whereas P_{870}^* and P_{680}^* are found in the purple bacteria and PSII only have midpoint potentials of −600 mV [20] and

☆ This article is part of a Special Issue entitled: Photosynthesis Research for Sustainability: Keys to Produce Clean Energy.

* Corresponding author at: Department of Biochemistry and Cellular and Molecular Biology, University of Tennessee, Knoxville, TN 37996, USA.
E-mail address: bbruce@utk.edu (B.D. Bruce).

0005-2728/$ – see front matter © 2013 Published by Elsevier B.V.
http://dx.doi.org/10.1016/j.bbabio.2013.12.013

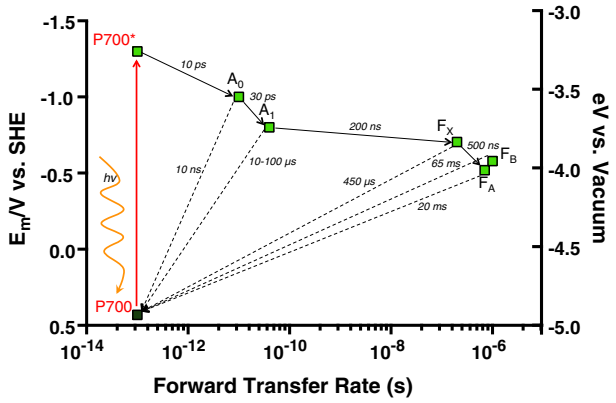

Fig. 1. Kinetics of electron transfer in PSI. After light excitation of P_{700} to P_{700}*, electrons travel downstream in energy to cofactors A_0, A_1, F_X, F_A, and F_B. Forward electron transfer lifetimes are shown (solid black arrows) on a log scale (x-axis) with the midpoint potential (mV) of the cofactors shown on the y-axis. Backward electron transfer (charge recombination) lifetimes are shown (dashed arrow) from cofactors back to P_{700}.

−650 mV [21], respectively. This more negative potential not only is a result of the chemical nature of the special pair but is also a consequence of the protein environment that coordinates these pigments and acceptors. The strong reductant produced by P_{700}* allows this reaction center to directly drive the reduction of protons into H_2 via a hydrogenase [22,23] or nanocatalyst [10,24,25].

These properties make PSI the source of the most powerful reductant in biological electron transfer [14,26–28]. It is this strikingly large negative midpoint potential that has attracted our lab and others to investigate the use of PSI as the preferred electron donor for applied photosynthetic purposes such as photosynthetic hydrogen production and photovoltaics [24,25,29–38]. Another interesting feature of PSI is the observation that the redox potential of the primary electron donor P_{700} special pair can vary considerably between organisms [39]. Using comparative biochemical analysis their work has demonstrated that P_{700} can have a potential that varies by over 70 mV. This work also suggests that the molecular environment of P_{700} may be quite responsive to bioengineering such that the energy levels of the primary charge separation may be "tuned" to the energy levels of either the electron donor or the electron acceptor. This ability to adjust the energy levels may be used to both enhance the kinetics of electron transfer as well as reduce the loss of free energy due to large over potentials. This potential versatility in electrochemistry will enable new, non-biological materials to be incorporated into future device design.

Finally, another attractive feature of PSI is the recent demonstration that the absorption properties of this reaction center can be varied based on the chlorophyll composition and the organism from which it is isolated. For example, it was shown in *Acaryochloris marina*, which contains predominately Chl *d*, the reaction center special pair P_{740} (most likely a dimer of Chl *d* [40]) is shifted ~40 nm to the red [41]. This finding would suggest that the discovery of more photosynthetic organisms would enable the optical properties of PSI to be further tuned. This is the precise design that has been invoked by a recent review by Blankenship et al. [42] where they propose that a two photosystem solar cell could be constructed to allow both the extraction of electrons from water via a PSII-like or biomimetic system and hydrogen production using a second, PSI-type reaction center. By shifting the absorption properties of PSI into the red region, these two photosystems will not compete for the same spectral region and will thus be able to harvest more of the solar spectrum, enabling a higher external quantum yield. It appears that PSI provides considerable variability both in its optical properties and in its redox potentials that may help facilitate future device design and optimization.

3. Structural advantages of using PSI in applied photosynthesis

3.1. Availability of high resolution structural data

Although the photosynthetic reaction center was the first membrane protein to have its structure determined in 1984 [43,44], it was nearly 20 years before the structure of PSI was determined at 2.5 Å [45] and several more years before the first PSII structure was determined [46]. Both photosystem structures were determined initially from thermophilic cyanobacteria, *Thermosynechococcus elongatus* or closely related organism *Thermosynechococcus vulcanus*. *T. elongatus* for example, has many advantages such as a fully sequenced genome, amenability to genetic transformation, and ability to undergo homologous recombination.

In most cyanobacteria the PSI complex is a trimer as shown in Fig. 2A. As a trimer, the MW of PSI is nearly a megadalton, and each monomer contains 12 subunits (PsaA–F, PsaI–M, PsaX) and many cofactors, including 22 carotenoids, 96 chlorophylls, 2 phylloquinones, 3 Fe_4S_4 clusters, 4 lipids, and ~200 water molecules. More recent work has indicated that the trimer may contain over 330 chlorophyll molecules [47]. In addition to the high-resolution X-ray structure of PSI, there are many TEM single particle structures [48,49] and even some high-resolution AFM structures of the PSI complex in native membranes [50,51].

Recently, time resolved crystallography has been performed using femtosecond X-ray protein nanocrystallography. This method uses very bright femtosecond pulses from a hard-X-ray free-electron laser to generate a large number of single-crystal X-ray diffraction patterns that each provides a "snapshot" of the protein as a function of time [52], which would allow the capture of millions of diffraction patterns from individual PSI nanocrystals. This technique also has the potential to avoid the significant problem of radiation damage characteristic of normal X-ray crystallography since the laser pulses are too short to generate degradation. This advantage is particularly attractive to photosynthetic complexes since they are particularly sensitive to radiation damage.

In addition to the cyanobacterial PSI complex, there have also been several structures determined from higher plants. The first structure from *Pisum sativum* var. Alaska was resolved to 4.4 Å resolution (Fig. 2B) [53]. A higher resolution was later achieved using a PSI complex from spinach to a resolution of 3.4 Å [54]. Both of these structures were part of a supercomplex that contained both the PSI reaction centers as well as four of the light harvesting complexes, LHCPa–d. Collectively, this complex contained 17 protein subunits, 168 chlorophylls, 2 phylloquinones, 3 Fe_4S_4 clusters and 5 carotenoids. Unlike trimers found in cyanobacteria, higher plant PSI complexes exist in nature as a monomer (Fig. 2).

Finally, there are many structures of the individual subunits made available by NMR or X-ray analysis, which provide insight into the structural determinants of redox potentials and/or the individual protein dynamics. These reports include the primary donor cytochrome c_6 [55], the soluble electron acceptors ferredoxin [56] and flavodoxin [57] and finally the individual stromal domain subunits PsaC [58], PsaD [59], and PsaE [60].

As a result of this abundance of X-ray, NMR, TEM, and AFM data, the opportunity to make highly tailored site-directed mutations and gene fusions is unsurpassed. This high level of structural insight combined with the ever expanding molecular genetic tools for gene editing [61–63] and the emerging tools for synthetic biology [64–66], provides researchers with a tremendously powerful toolkit for manipulating PSI for applied photosynthesis.

3.2. Surface access to electron acceptors

Regardless of the oligomeric nature of PSI, a common feature is the presence of an extramembraneous domain known as the "stromal

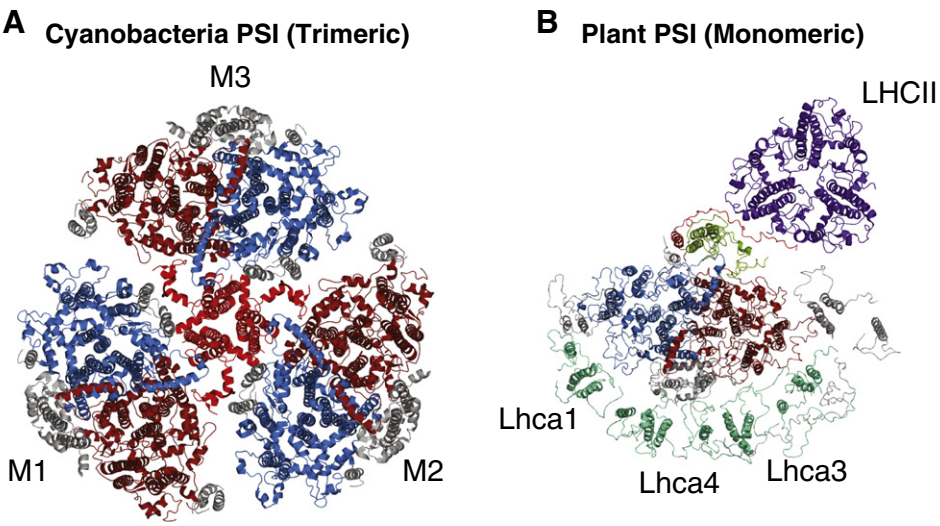

Fig. 2. PSI crystal structures. (A) PSI from cyanobacteria (*Thermosynechococcus elongatus*, PDB ID: 1JB0). M1-3 denotes individual monomers comprising the native trimer. Major subunits are shown: PsaA (burgundy), PsaB (blue), PsaL (red), and other subunits (gray). (B) PSI from plant (*Pisum sativum*, PDB ID: 2001). LHCI subunits are shown in teal (Lhca1-4) and LHCII in violet. Major subunits are shown: PsaA (burgundy), PsaB (blue),PsaL (olive), PsaH (red), and other subunits (gray).

hump". This domain protrudes out from the membrane and is composed of three subunits, PsaC, PsaD, and PsaE. These subunits are composed of loosely packed beta strands and some short alpha helices, yet none of the subunits contain a membrane spanning element as shown in Fig. 3. Fig. 4A–D shows that this domain is quite similar in both cyanobacteria and higher plants.

Unlike the Type II reaction centers in purple bacteria and PSII, the organization of the cofactors associated with electron transfer (specifically F_X, F_A and F_B) is quite close to the surface of PSI permitting rapid electron transfer to the soluble electron transfer components ferredoxin and flavodoxin [67]. As shown in Fig. 3A–D these iron sulfur centers are in close proximity to the surface of PSI. In fact the FeS centers from both F_A and F_B are within 5–11 Å from the surface throughout the stromal hump. This close distance will allow relatively rapid electron transfer to a host of acceptors including not only the native electron acceptor, ferredoxin/flavodoxin [67] but also non-native electron acceptors such as MV [68] organic semiconductors such as C_{60} [69]and inorganic semiconductors such as TiO_2 and ZnO [33]. Some of these electron acceptors are schematically shown in Fig. 5.

An additional advantage of the non-membrane spanning nature of the stromal hump is the relatively straightforward means to replace these subunits in vitro. This design feature of PSI provides many opportunities for further bioengineering since these subunits can be both easily removed and replaced using *Escherichia coli* expressed proteins in vitro (PsaC, PsaD and PsaE) [70–73]. This may allow the powerful tools of synthetic biology in *E. coli* to be applied to PSI without having to develop an entirely new synthetic biology toolkit for a photosynthetic organism. In addition, certain mutations or subunit modifications that may disrupt the photosynthetic process in vivo may still be obtained via this in vitro re-assembly process, as was recently demonstrated with the introduction of ZnO and TiO_2 binding domains to PsaD and PsaE of *T. elongatus* [12]. However, it may still be preferred to have an in vivo method of making these changes since the process of re-assembly may never be complete and could lead to heterogeneity in the PSI complex, lowering the efficiency of a device.

3.3. Interaction with diverse electron donors

Although both PSI and PSII accept electrons from their lumenal surface, PSI is distinct in that it is quite promiscuous in terms of a viable electron donor. P_{680} in PSII, upon photo-oxidation, receives its electrons from the oxygen-evolving complex that is attached peripherally to the lumenal surface. Although this enables water to function as the electron donor to PSII, it is also a relatively labile system, which is easily photodamaged with a high turnover rate and must be repaired frequently [74,75]. PSI on the other hand is much more robust and can also accept electrons from a wide range of proteins including the native electron donors, cytochrome c_6 and plastocyanin [76], organic redox compounds such as dichlorophenol indophenol (DCPIP) [77], synthetic redox-active organometallic complexes such as $Os(bpy)_2Cl_2$ [78], Au surfaces [79], self assembled alkanethiols attached to Au [80], and graphene [81].

This ability to accept electrons from a diverse set of donors is shown schematically in Fig. 5, and we demonstrate the re-reduction of P_{700} using some of these various donors after photobleaching via flash photolysis (Fig. 6). However, in many cases these systems need to be in a high molar excess to keep up with the rapid electron transfer reactions with PSI. Future works will fine-tune both the electrochemistry and the interactivity of these systems to facilitate the highest PSI turnover with the least energy loss due to an over potential.

3.4. Availability of multiple oligomeric forms

Interestingly, unlike the non-oxygenic, monomeric bacterial reaction centers, photosynthetic reaction centers in oxygenic organisms are found as monomers (plant PSI), dimers (all PSII), trimers (most cyanobacterial PSI), and tetramers (few cyanobacterial PSI). Cyanobacterial PSI trimers have been reported in many published works [49,82–92], and the only existing crystal structure of a cyanobacterial PSI, from *T. elongatus* BP-1 (*T. elongatus*) [93], suggests that cyanobacterial PSI preferentially forms a trimer. Supporting this idea is the observation that cyanobacterial PSI trimers have been reported in almost every subclass of cyanobacteria. The most well characterized PSI trimers are from *Synechocystis*, *Synechococcus*, and *Thermosynechococcus*, where PsaL is needed for PSI trimerization in these cyanobacteria [94–97]. In contrast, plant PSI is monomeric in the presence of PsaL, possibly due to interaction with the PsaH subunit that is not found in cyanobacteria [98–100]. The fact that PSI can come in two oligomeric states (monomer and trimer) provides an advantage for increasing the density of PSI in a device. The trimer yields a very high local concentration, yet due to its high molecular weight, high coverage or penetration will be difficult. By using both the trimer

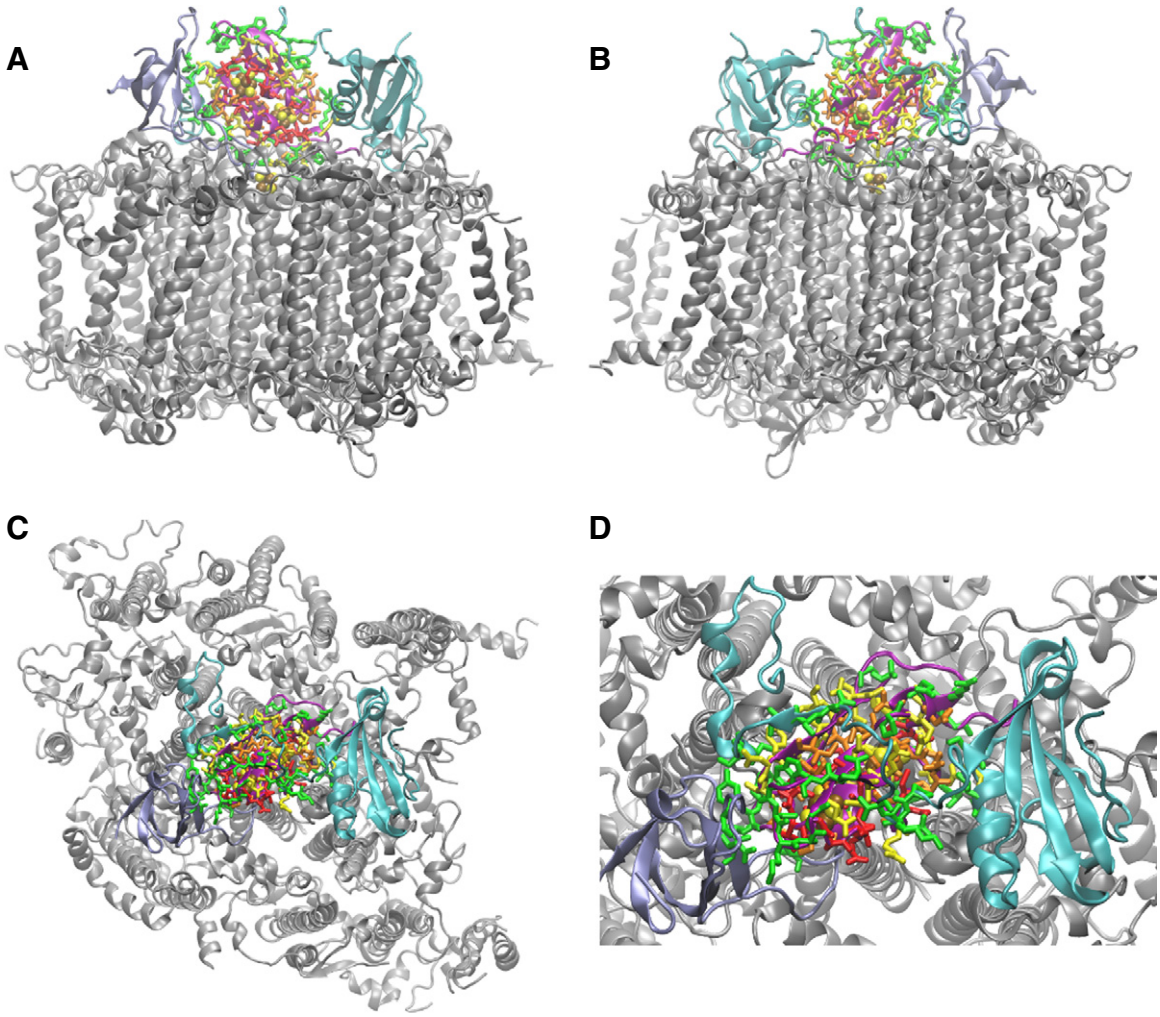

Fig. 3. Accessibility of stromal iron–sulfur clusters. Backbone of Photosystem I is represented in cartoon-ribbons with emphasis on the stromal subunits PsaC (purple), PsaD (cyan), and PsaE (blue). The inorganic electron transfer components forming the end of the internal electron transport chain are cubane [4Fe–4S] clusters, Fa and Fb, and are represented in space-filling and colored by element Fe and S in brown and yellow respectively. Amino acids proximal to the clusters are represented as follows: AA's with α carbon ≤5 Å, >5–7 Å, >7–9 Å, or >9–12 Å from Fa or Fb are in red, orange, yellow and green respectively. A.) PSI complex as seen from plane of thylakoid membrane facing "exposed" side of stromal subunits. B.) PSI observed from membrane plane facing the "protected" side of the stromal subunits. C.) View of PSI from stromal side of the normal of membrane plane. D.) Detail view as in C, with "protected" side facing upward and "exposed" side facing downward.

and monomer forms of PSI, it may be possible to get increased coverage as demonstrated in Fig. 7. This configuration shows a random deposition of PSI trimers on a gold surface that is then further treated with a second deposition of PSI monomer, increasing the coverage by 35%.

4. Thermotolerance and extended stability

One of the advantages of PSI is the availability of well-characterized and easily cultivated thermophilic strains of cyanobacteria such as *T. elongatus* [101]. This organism is capable of growth at temperatures up to 60 °C and was the source of the first crystal structure for PSI [45]. In addition, this protein complex has been shown to have a thermotolerance of up to 70 °C based on the protein structure as reflected by circular dichroism spectrometry [10]. This extreme thermal tolerance may be an attractive trait when PSI is integrated into various solid-state devices or solar cells that may be subject to high temperatures during illumination. Moreover, it has been shown that PSI isolated from both cyanobacteria and plants remains photochemically active in a solid state for over 21 days [102], in an aqueous hydrogen producing bioreactor for over 85 days [10], and in a wet electrochemical cell for over 280 days [103]. It should be noted that in both of these studies the activity of the PSI complex was nearly unchanged after months of continuous testing. This robust stability makes it very difficult to estimate the true functional longevity and stability of PSI, however it is expected that it will be affected by various conditions including spectral variations, light intensity, and temperature [11].

5. Established ability to genetically engineer PSI in cyanobacteria

Oxygenic photosynthesis is the primary energy source on Earth, capturing solar energy via absorption by Chl *a*/*b*, with water photolysis as the electron donor providing reducing equivalents for the fixation of atmospheric levels of CO_2 into hydrocarbons. Cyanobacteria, commonly called blue/green algae, containing only Chl *a*, are the only prokaryotes capable of using solar energy to support oxygenic photosynthesis. As prokaryotes, most of the well-established genetic tools of bacterial genetics are applicable to cyanobacteria, making it considerably easier to genetically engineer than eukaryotic photosynthetic organisms such as green algae and plants. With this advantage, considerable progress has been made over the past thirty years to engineer many strains of cyanobacteria including but not restricted to the model organism *Synechocystis* PCC #6803 [104–106]. More recently, however,

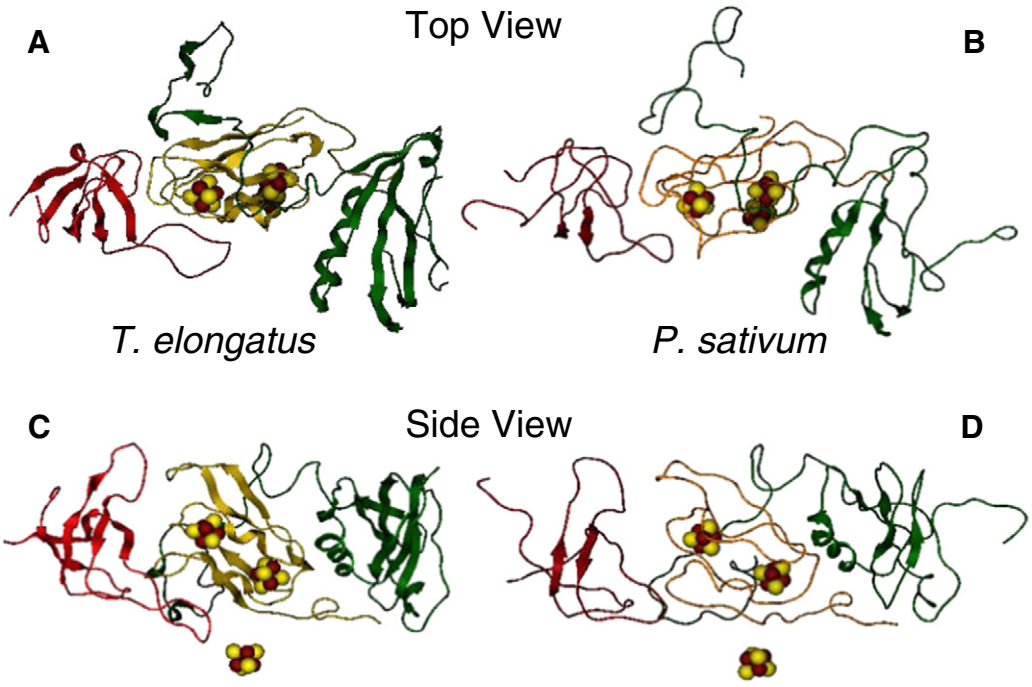

Fig. 4. Crystal structure of PSI's "stromal hump" in cyanobacteria and plants. A&C show the top (from stroma) and side view of the stromal subunits (PsaC—yellow, PsaD—green, PsaE—red) from *Thermosynechoccocus elongatus* (1JB0). B&D shows the same subunits in *Pisum sativum* with the same color scheme. The FeS clusters are shown with F_B furthest to the left.

the powerful tools of molecular and synthetic biology have been directed to bioengineering cyanobacteria for a host of new bioenergy and environmental applications, including biohydrogen production [107–112], advanced CO_2 sequestration [113], production of next generation biofuels [114–117], and various bioactive/value-added compounds [118–120].

Not surprisingly, one of the first areas to attract the application of molecular biology and genetic engineering of cyanobacteria was the ability to perform gene knockouts, gene replacement and site-directed mutagenesis [121–123]. These techniques were broadly applied to the analysis of the photosystems and in particular Photosystem I which demonstrated the robust ability to be manipulated. For example, nearly all of the PSI subunits have been either deleted or genetically altered in some form including PsaA/B [124,125], PsaC [126–128], PsaD, PsaE [129,130], PsaF [131,132], PsaI [133], PsaJ [134,135], PsaK [136], PsaL [122] and PsaM [136]. In addition, there has been considerable effort to optimize both the interactions with the primary donors cytochrome c_6 and plastocyanin [137] and the terminal acceptor ferredoxin [138]. Future work on integrating PSI into photovoltaic devices will require progress in bioengineering to facilitate specific attachment of the reaction centers to different types of surfaces, including semiconductors and catalysts [139,140].

6. PSI surface immobilization

The integration of redox proteins such as PSI into photoelectrochemical devices requires immobilization strategies that ideally would allow direct electron transfer between the electrode and protein's active site(s) (e.g. PSI's P_{700}/F_B). Due to the dipole nature of PSI, proper orientation on and proximity to the electrode surface appear to be essential factors in attachment design. The conductive and semiconductive substrate surfaces used for PSI depositions have evolved from the widely used Au to other materials including, TiO_2, ITO, glass, ZnO, alumina, and graphene.

The most commonly utilized strategies often involve the usage of organothiol-based self-assembled monolayers (SAMs). For attachment of PSI, SAMs can be terminated or functionalized with mercaptoacetic acid/2-mercaptoethanol [141], nitrilotriacetic acid (NTA) [69], alkanethiols [37,79,80,142], terephthaldialdahyde (TPDA) [143–145], 3-mercapto-1-propanesulfonic acid [146,147], aminoethanethiol [145,148], and pyrroloquinoline quinone [149]. Because of the highly variable design and attachment chemistries, we briefly summarize the studies utilizing these variations below:

6.1. PSI on (Au)-based SAMs

Lee et al. 1997 [141]: Tested –OH, –COOH, and –SH terminated SAMs to immobilize and control the orientation of 2D spatial arrays of PSI on Au surfaces. They found that –OH terminated SAMs gave the most desired, perpendicular orientation of PSI.

Das et al. 2004 [69]: To achieve oriented PSI assembly, recombinant PsaD–His_6 was immobilized on Ni^{2+}–NTA functionalized Au surface. This then was exposed to native PSI complexes where the intrinsic PsaD subunit naturally exchanged with an excess of the recombinant PsaD–His_6, resulting in immobilization of PSI with P_{700} facing away from the ITO/Au substrate. Peptide surfactants were also used to increase PSI stability during and after assembly.

Ko et al. 2004 [79]: Examined the PSI to *ω-functionalized* and *n-alkanethiols* gold surface adsorption based on surface composition. They concluded that the PSI-solubilizing agent, Triton X-100, adsorbs to low-energy surfaces (hydrophobic SAM), and the PEG groups of the Triton layer are very resistant to protein adsorption. This inhibiting effect can be prevented by the addition of a more active surfactant (e.g. dodecanol).

Frolov et al. 2005 [150]: Various cysteine mutations were made to residues on the lumen exposed face of PSI to allow for direct thiol coupling to the Au surface. Even with the mutations being placed in an increasing distance from the P_{700} site, PSI attachment was achieved with all mutants, suggesting that a specific location is not required as long as the cystein is on an extramembranal loop of PSI's lumenal surface.

Kincaid et al. 2006 [80]: In an attempt to mimic the natural thylakoid membrane that surrounds PSI, this group immobilized PSI using HOC_6S/Au SAMs followed by a backfilling step to adsorb longer-chained methyl-terminated alkanethiols in the interprotein domains to displace the shorter, more unorganized HOC_6S monolayer.

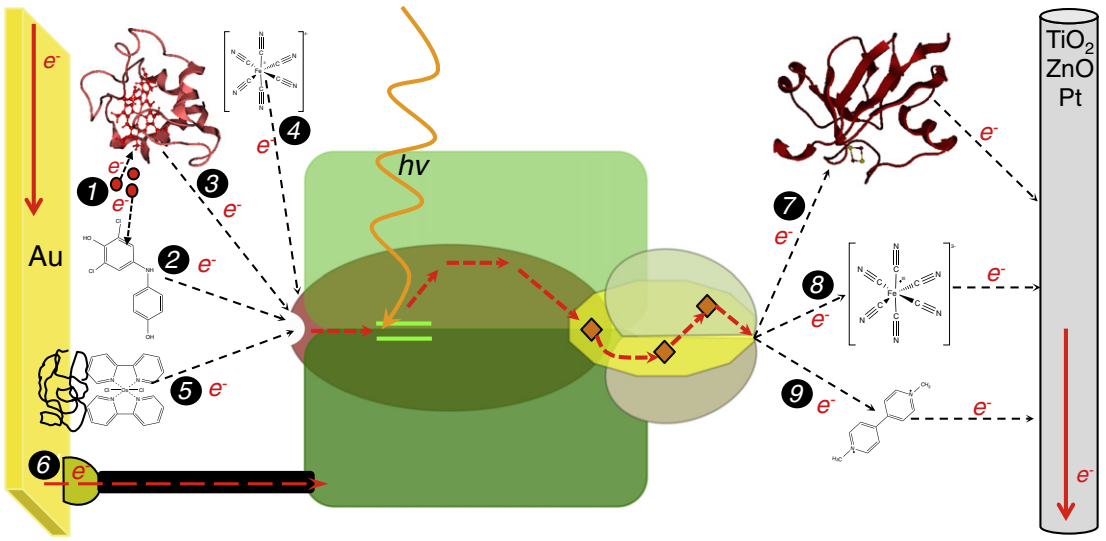

Fig. 5. Biohybrid schemes integrating PSI with various electron transfer mediators. Soluble mediators (2) DCPIP, (3) cytochrome c_6, (4) $[Fe(CN)_6]^{4-}$, or (5) $Os(bpy)_2Cl_2$ can be reduced by Au electrode or (1) sodium ascorbate, allowing the electron transfer to (6) immobilized PSI. PSI can also be directly reduced by immobilization wire (6) (NTA–Ni–His_6–PSI). Soluble acceptors (7) ferredoxin, (8) $[Fe(CN)_6]^{3-}$, or methyl viologen can be used to transfer electrons from the F_B Fe–S center of PSI to TiO_2, ZnO, or Pt electrode.

Ciobanu et al. 2007 [142]: PSI adsorbed on hydroxyl-terminated hexanethiol (HSC_6OH) modified gold substrate showed an enhanced reduction current for P_{700}^+ in the presence of light and methyl viologen. They also saw that HSC_8OH terminated SAMs formed a more ordered monolayer than the HSC_6OH monolayer. They were able to analyze PSI functionality after adsorption by cyclic voltammetry, looking at signals of F_A, F_B, and P_{700}.

Faulkner et al. 2008 [143]: To address the issue of the labor intensive and time consuming procedures required in previous studies to adsorb PSI to SAMs, this group demonstrated that a vacuum-assisted method can produce dense, oriented monolayers of PSI about 80 times faster than the traditional solution adsorption techniques. This vacuum-assisted method also enabled PSI assembly on other surfaces that were resistant to protein adsorption.

Ciesielski et al. 2008 [144]: PSI was immobilized on the surface of nanoporous gold leaf (NPGL) electrodes via covalent bonds between the aldehydic groups of the TPDA-functionalized NPGL SAM and the exposed lysines on PSI. The resulting photocurrent from the electrodes was shown to be dependent on irradiating light intensity and dealloying times of the electrode production.

Terasaki et al. 2009b [147]: PSI was bound on an Au/3-mercapto-1-propane-sulfonic acid-SAM by electrostatic interactions. They were able to show the ability of the PSI–Au electrode to act as a gate film in FET sensoring for imaging devices.

Mukherjee et al. 2010 [31]: The deposition of PSI onto hydroxyl-terminated alkanethiolate SAM/Au substrates was investigated with the goal of having better control of the assembly morphology. They showed that a lower PSI concentration, via electric-field deposition, minimizes PSI aggregation while providing a more uniform coverage onto the surface as compared to gravity-driven deposition methods.

Ciesielski et al. 2011 [145]: Dense monolayers of PSI were immobilized to aminoethanethiol terminated SAMs functionalized with TPDA (similar to that of Ciesielski et al. [144]). A mechanistic model was developed for PSI immobilized SAMs, in which kinetic and electrochemical parameters were used to predict photocurrent densities. Discrepancies between simulated and experimental current densities were discussed, along with a predicted conclusion that unless at least 80% of the PSI was oriented the same way, the majority of the photocurrent is nullified.

Mukherjee et al. 2011 [32]: Various immobilization conditions of PSI onto SAM/Au substrates were tested. Conditions tested included adsorption temperature, monomeric/trimeric forms of PSI, and type of detergent used. A comparison was also made on the immobilization characteristics when applying a gravity driven versus an electric field

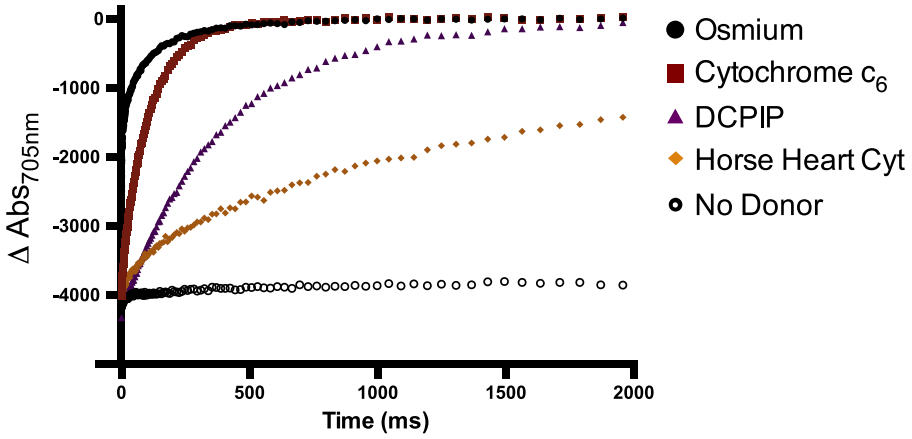

Fig. 6. PSI-P_{700} reduction by various donors. *Thermosynechococcus elongatus* PSI (30 nM) electron transfer rates were measured with a LED pump-probe spectrometer (Joliot Type Spectrometer, JTS-10), detecting at 705 nm. Donors individually tested include $Os(bpy)_2Cl_2$ (2 nM), recombinant *T. elongatus* cytochrome c_6 (300 nM), DCPIP (1.2 μM), and horse heart cytochrome (1 mM). Reaction mix also included 2 mM sodium ascorbate and 1 mM methyl viologen, and 0.03% n-Dodecyl-β-D-maltoside in MES buffer (pH 6.4).

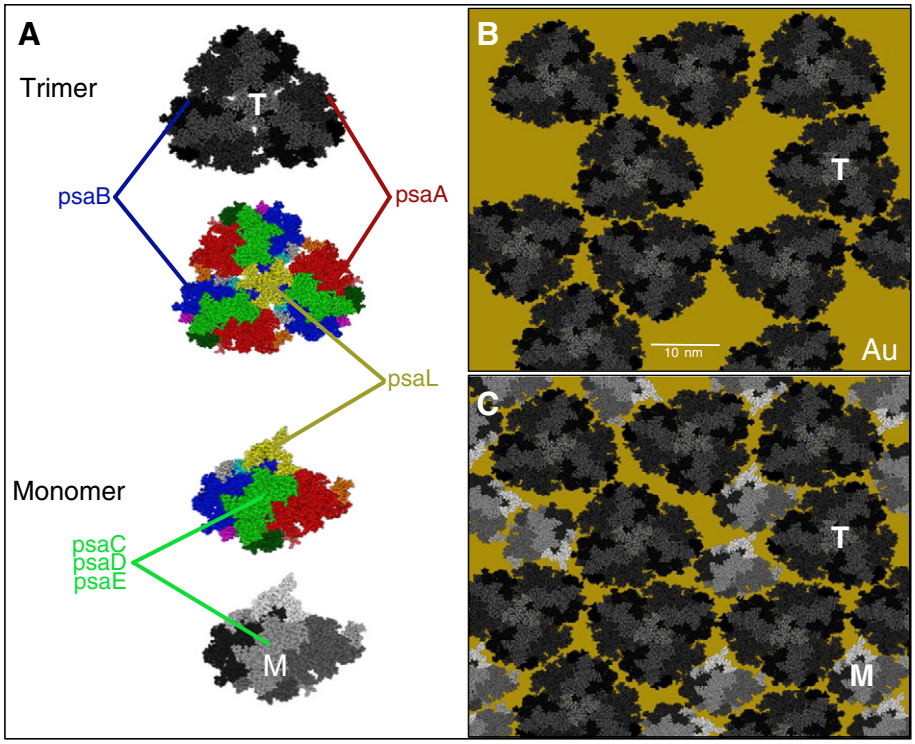

Fig. 7. Proposed improved surface coverage using electrodeposited trimers and monomers. (A) Labeling of PSI subunits: Core subunits PsaA (red) and PsaB (blue); stromal subunits PsaC, PsaD, and PsaE (green); and PsaL (yellow). (B) An example of a random and arbitrary deposition of PSI trimmers on an AU SAM is shown with 60.2% coverage. (C) The pattern in B was further treated to a random deposition of the PSI monomers yielding an increase in coverage to 84.0%. Pixel calculations were done with ImageJ and PDB *Thermosynechococcus elongatus* PSI crystal structure (1JB0) was constructed with MOE software.

assisted assembly technique. This study provided one of the few direct demonstrations of the uniform orientation of PSI by using an immunofluorescent detection strategy. This analysis can both provide a method to quantitate the attachment density and confirm the predicted orientation based on the strong PSI dipole.

Efrati et al. 2012 [149]: CdS quantum dots (QDs) and PSI, immobilized onto a pyrroloquinoline quinone (PQQ) monolayer linked to Au electrodes were compared based on their anodic/cathodic switchability of the photocurrents in the presence of different photoelectrochemical configurations. They concluded that upon irradiation under O_2, the two systems gave rise to a potential-induced control of anodic and cathodic directions in photocurrent.

Manocchi et al. 2013 [37]: By using an electrophoretic deposition procedure, PSI assembly on alkanethiol SAMs was enhanced, and the immobilized PSI density was easily controlled. SAM surface charge composition, specifically MHO and MHA, greatly increased the amount of bound PSI. This work demonstrated that there is some interaction between the terminating group of the SAM and some surface property of PSI. The stability of the PSI/SAM electrode was shown to be maintained for a minimum of 3 h with illumination.

6.2. Other metal/conductive surface-SAMs

While gold has been the main conductive surface used in the above studies, other materials like gallium (III) arsenide (GaAs) [151], titanium oxide (TiO_2) [152], silicon (Si) [142], and graphene [81] have also emerged as a suitable and attractive material for PSI devices.

Frolov et al. 2008b [151]: Cysteine mutant PSI was chemisorbed to maleimide-functionalized GaAs SAMs. The dry-oriented junction allowed for a non-aqueous system, and was still functional after one year.

Nikandrov 2012 [152]: PSI was immobilized in a mesoporous TiO_2 semiconductor matrix. The larger pore diameter of the TiO_2 matrix allowed for a high concentration of PSI to be immobilized, thus allowing the complex to absorb high light.

LeBlanc et al. 2012 [142]: Conducted a systematic study on how both n- and p-doped silicon can increase the photocurrent density of PSI films. By comparing silicon doping types and densities, they concluded that heavily p-doped silicon provided the best surface for PSI attachment and photocurrent generation.

Gunther et al. 2013 [81]: First group to exploit the transparent and highly conductive properties of graphene in PSI attachment. Graphene's transparency is noted to be very attractive for the usage of high concentrations of opaque mediators.

6.3. Carbon nanotubes/nanoparticles

While the previous studies looked at PSI functionality as a monolayer on a planar substrate surface, other works have investigated the potential enhancement in photocurrent by utilizing (3D) nanostructured electrodes that provide an increased surface area, consequently allowing for a greater deposition of PSI particles. These nanostructured substrates such as nanoparticles (NPs) [153], nanowires [33], and nanotubes [154,155] have been used for PSI attachment and increased photocurrent in the following studies:

Terasaki 2006 [153]: Constructed PSI–gold nanoparticle hybrid electrodes, by depositing gold NPs onto a planar gold substrate followed by SAM formation by MPS. PSI was then electrostatically adsorbed to the MPS modified electrodes.

Carmeli et al. 2007 [154]: Used cysteine mutants of PSI to bind maleimide modified carbon nanotubes (CNTs) through a chemical process on a gold electrode. Variations of this process also allowed

for the construction of cross-junctions between two CNTs by a PSI connection.

Kaniber 2010 [155]: Three different strategies for on-chip functionalization of CNT–PSI hybrids were demonstrated. The covalent attachment utilized cysteine mutant PSI bonding to maleimide functionalized CNTs. The second method proposed a hydrogen bond formation between the amino groups of the ethylenediamine functionalized CNT and cysteine mutant PSI treated with dithiothreitol. The final method exploited the electrostatic forces between the positively charged regions on PSI and the CNTs negatively charged terminal groups.

Mershin 2012 [33]: PSI was attached to two semiconducting substrates (TiO_2 and ZnO). PSI was physisorbed to TiO_2 on FTO coated glass and self assembled on ZnO nanowires with a PsaE–ZnO replacement strategy.

6.4. Other PSI assemblies (multilayers, sol–gels, and redox polymers)

Aside from deposition of PSI monolayers directly onto surfaces, the following works have demonstrated improved functionality, stability, and photocurrent generation with the incorporation of PSI multilayers, sol–gels, and redox polymers into their device fabrication schemes:

O'Neill and Greenbaum 2005 [156]: PSI was immobilized onto a clear organosilicate glass reacted with a colloidal sol solution (sol–gel). This sol–gel matrix, while enabling the entrapment of PSI, also offered a stabilizing environment for other biomolecules such as redox mediators, allowing their chemical reactivities to be retained. In addition, the transparent nature of the matrix is an obvious advantage in applications requiring full optical functionality of the photoactive biomolecules.

Frolov et al. 2008a [150]: Serially-oriented multilayers of PSI were assembled on an Au electrode. This assembly was created with a mutant PSI containing a lumen-exposed cysteine, which formed a sulfide bond with Au to form the first layer. Platinum was then deposited to the stromal face of PSI, allowing for the sequential layer of mutant PSI to form a sulfide bond with the platinum patches. The highest photovoltage was achieved with the multilayer of Au–PSI–Pt–PSI–Pt–PSI.

Ciesielski et al. 2010 [103]: Developed a photoelectrochemical cell with multilayer assembly of PSI. A PSI suspension and liquid electrolyte was injected into a reservoir held between a gold cathode and a Cu-modified ITO anode.

Ciesielski et al. 2010b [148]: By mimicking stacked thylakoid structures, multilayers of PSI were formed through sequential deposition of a liquid PSI suspension onto gold and glass substrates via a vacuum-assisted assembly. PSI deposition of up to 7 layers was shown to have a matching increase in absorption intensity and photocurrent generation.

Kopnov et al. 2011 [157]: Tested the combinations of coupling PSII and PSI in order to enable electron flow from water splitting at PSII to reducing P_{700} of PSI. The variations included one protein in solution and the other sol–gel encapsulated, both in solution, or both sol–gel encapsulated. These implementations offered a simple solution to the challenging task of utilizing both photosystems in the same device, allowing the usage of water as the sacrificial electron source.

Toporik 2012 [158]: PEG-treated PSI crystals were immobilized onto ITO coated glass slides. Although photocurrent densities were not reported, large photovoltages (~50 V) were seen, which would be the largest reported for any inorganic material device. This anomalous value was proposed to be a result of "electron trapping in deep centers in the vicinity of the F_B acceptor", due to the packing and alignment of PSI's dipole in the crystallized state.

Yehezkeli 2013 [159]: The redox polymer, poly-benzyl viologen (PBV2+) was employed as an "interprotein glue" in the layered assembly of PSI on a transparent ITO electrode. Increasing photocurrent was seen with the sequential addition of PSI–PBV layers up to a maximum of 3 layers.

7. PSI stabilization/enhancement

While enhancements have been made to increase photocurrent via surface modifications, variable redox mediators, and increased PSI packing densities, it is also crucial to retain PSI's optical functionality for an extended period of time in order for the device to be practical. The following approaches tried to address the main issue of PSI's hydrophobic domains being unnaturally exposed on the surface, causing rapid protein degradation. In this regard, Kiley et al. [29] studied the effects of various peptide detergents on PSI stability and function. They saw that the designed peptide detergent, acetyl-AAAAAAK (A_6K), stabilized PSI for at least 3 weeks in the dry form. This discovery followed some initial studies with peptide surfactants done by Das et al. [69]. Along this line, Matsumoto et al. [30] studied a new class of designer peptide surfactants (ac-I6K2-CONH2, ac-A6K-CONH2, ac-V6K2-CONH2, and ac-V6R2-CONH2). They concluded by offering a guide to designing future peptide surfactants for optimal stabilization of active PS-I. The four main factors included: 1) an acetylated N-terminus 2) a short hydrophobic tail consisting of 6 consecutive hydrophobic residues 3) 1-2C-terminal positively charged polar residues and 4) an amidated C-terminus [30]. Another approach taken by Kincaid et al. [80] attempted to mimic the natural thylakoid membrane that surrounds PSI. After the immobilization of PSI using HOC_6S/Au SAMs, they added a backfilling step to adsorb longer-chained methyl-terminated alkanethiols in the interprotein domains to displace the shorter, more unorganized HOC_6S monolayer.

The previous studies have analyzed PSI stability with techniques probing for its optical properties, such as steady-state emission spectra [29], fluorescence spectra [69], and reflectance absorption infrared spectroscopy [80]; however Gerster et al. [160] were able to look at the photocurrent generated by a single PSI molecule immobilized on an Au surface. The immobilization of PSI between the substrate and the metallized scanning near-field optical microscopy (SNOM) tip was achieved with PSI cysteine mutations and the ability to control SNOM tip to substrate distance by a high-resolution piezoelectric element.

Along with stabilizing and maintaining PSI's native optical properties, increasing the range of its absorption spectra has also been of interest. Although having a quantum efficiency nearing unity, PSI is still limited to absorbing about 1% of natural sunlight. Carmeli et al. [161] were able to enhance PSI's light absorption capability with the attachment of colloidal metal (gold and silver) nanoparticles, which acted as optical antennas to functionalize more of the spectrum to photons for P_{700} activation. They also described a new method that enables a higher yield of PSI attachment to NPs.

8. Diffusible redox mediators/molecular wires

While the native donors to PSI are metalloproteins (plastocyanin or cytochrome c_{553}), the majority of these works employ the combination of sodium ascorbate (NaAs) and 2,6-dichlorophenolindophenol (DCPIP) to transfer the electron from substrate surface to PSI where NaAs acts to keep a reduced pool of DCPIP for P_{700} reduction [103,143,144,146,153,162–164]. The following complexes have also been used for electron donation to PSI: reduced ferricyanide $K_4Fe(CN)_6$ [148], osmium complexes ($Os(bpy)_2Cl_2$) [37,78], Z813

Co(II)/Co(III) electrolyte [33], and ruthenium hexamine trichloride (RuHex) [81].

In many studies an electron acceptor has also been used to prevent the charge recombination reaction of electron flow from F_B back to P_{700} and transferring electrons to the opposing electrode. With a midpoint potential of (−0.446 V vs SHE), methyl viologen (MV) has been widely used to accept electrons from PSI F_B (−0.58 V vs SHE) [37,78,142,147]. Other notable acceptors used include a naphthoquinone-derivative (NQC_{15}) [146,162], oxidized $K_3Fe(CN)_6$ [148], and methylene blue [81]. Ciesielski et al. [148] showed that $Fe(CN)_6$ was able be used as both donor and acceptor, minimizing ET components by oxidizing $[Fe(CN)_6]^{4-}$ to $[Fe(CN)_6]^{3-}$ at the lumenal P_{700} interface and reducing $[Fe(CN)_6]^{3-}$ to $[Fe(CN)_6]^{4-}$ at the stromal F_B site.

After P_{700} photo-excitation, electron transfer follows the scheme of $P_{700} \rightarrow A_0 \rightarrow A_1 \rightarrow F_X \rightarrow F_A \rightarrow F_B$, with these active cofactor sites buried deep within PSI. The wiring of PSI to a substrate via an electron transfer cofactor was attempted by Terasaki et al. [162], where the A_1-phylloquinone was extracted and reconstituted with a naphthoquinone-derivate (NQC_{15}) attached to Au NP. The NQC_{15} molecular wire has a very similar length as the native A_1, allowing the Au NP to be attached near the PSI surface. This NQC_{15}S–Au(NP)–PSI was then immobilized with an Au – S bond via a SAM of 1,4-benzenedimethanethiol. By wiring the A_1 cofactor of PSI's electron transfer chain to the substrate surface, the direct electron transfer was achieved from A_1 to the electrode while bypassing the FeS clusters (F_X, F_A, F_B) in the stromal hump of PSI. DCPIP and NaAs were also used for electron donation to P_{700}. This group further improved on this method with an A_1 replacement using a naphthoquinone-viologen linked compound ($NQC_{15}EV$), where the viologen had the appropriate redox potential (−0.446 V vs SHE) to mediate electron transfer through the wire from A_1 (−1.05 V vs SHE) [146]. The use of methyl viologen at the end of the NQC_{15}, instead of an Au NP, increased the photocurrent by about 25 times as shown in Table 1. With these two studies, Terasaki et al. were able to demonstrate that electron transfer to an electrode is possible via a direct connection from a PSI cofactor (A_1), utilizing either a conductive metal NP (Au) [162], or an electron mediator (MV) [146].

Miyachi et al. followed up on this A_1-phylloquinone replacement method with a study that demonstrated how the addition of two surfactants enhanced the sensitivity of the NQC_{15}S–Au(NP)–PSI system by enabling electron storage in the AuNPs [165]. This group also implemented a terpyridine-terminated naphthoquinone, allowing for a connection to Co(II) ions to form the complex of PSI_tpy–C_{15}NQ_ITO [166]. The development of these new strategies has contributed to the immobilization of PSI on surfaces for applications in both photovoltaic cells and photosensing devices.

9. Photocurrent production

As seen in Fig. 8, much progress has been achieved in enhancing PSI-photocurrent density since the early 2000's. In less than a decade, over 30 papers have been published reporting various activities of PSI. From these papers, the reported photocurrent density, when normalized to excitation intensity, has jumped up almost 4 orders of magnitude from 0.48 [153] to 4469 [33] ($\mu A\ cm^{-2}\ mW^{-1}$). Although it might be impossible to pinpoint all the subtle changes made in fabricating PSI-biohybrid devices during this time, along with their individual levels of contribution toward increasing photocurrent yield, some significant factors are evident.

The combination of NaAs/DCPIP has been the most widely used electron source and donor for these systems. Aside from two studies [103,163], all others utilizing NaAs/DCPIP achieved less than 2 $\mu A\ cm^{-2}$ in photocurrent generation. The two exceptions from Frolov et al. [163] and Ciesielski et al. [103] both assembled a multilayer of PSI, while the others had just a monolayer deposited. Even with a photocurrent of 2 $\mu A\ cm^{-2}$, Ciesielski et al. had used twice as much DCPIP (5 mM) as any other study [103]. Although probably one of the most cost effective PSI donors, DCPIP proves to be a limiting factor in photocurrent production as it is considered a much poorer electron donor to PSI compared to native metalloproteins or other artificial complexes.

Potassium ferricyanide was implemented as both electron donor to P_{700} and electron acceptor from F_B with a continuous redox cycle from $[Fe(CN)_6]^{4-}$ to $[Fe(CN)_6]^{3-}$ at P_{700} and $[Fe(CN)_6]^{3-}$ to $[Fe(CN)_6]^{4-}$ at F_B to produce an enhanced photocurrent of 7.9 $\mu A\ cm^{-2}$ [148]. This can prove to be a fairly attractive feature for large-scale implementations, as it would minimize the input to drive the reaction. The metal osmium (Os), considered the densest stable element [167], has also been used recently both as an immobilization matrix and electron donor in the form of an "Os-complex modified polymer" [78] and as an ET mediator, $Os(bpy)_2Cl_2$, sitting atop alkanethiol-SAMs [37]. While the Os-complex polymer gave an enhanced photocurrent of 29 $\mu A\ cm^{-2}$ [78], osmium is also the least abundant of the stable elements [168] and therefore not practical for large-scale applications. Though synthesized and tested originally for dye-synthesized solar cells [169], the Co(II)/Co(III) ion-containing electrolyte Z813 was used with PSI to generate one of the highest (highest if normalized to excitation intensity) photocurrents of 362 (4469-normalized to mW^{-1}) $\mu A\ cm^{-2}$ [33]. This significant increase in photocurrent, if attributed to Z813, shows a tremendous potential for the usage of synthesized redox mediators instead of relatively expensive rare metals.

While the majority of electrode surfaces and immobilization schemes used with PSI involve SAMs on an Au surface, we will discuss the variation in strategies implemented by the top performers. A noticeable trend in enhanced photocurrent generation with values of 2 [103], 7.9 [148], and 120 [163] $\mu A\ cm^{-2}$ is seen in the assembly procedures that utilize a multilayer of PSI instead of a single immobilized monolayer. Amongst these works, there appears to be a noticeable trade-off between PSI orientation within the multilayer and the generated photocurrent. With the two lower values achieved by the Ciesielski group, PSI multilayer depositions were made without bias to PSI's dipole orientation in relation to the surface electrode. On the other hand, the device that generated a 10-fold higher photocurrent by the Frolov group was constructed with cysteine mutant PSIs that allowed for subsequent attachment of Pt patches between each PSI layer. Whether or not the cost of the added steps in generating mutant PSIs and the application of expensive platinum salts is worth the 10-fold increase in photocurrent is debatable.

In looking at the two recent reports that generated the highest photocurrents ever produced by a PSI-based device [33,139], we notice the unique surfaces used for PSI immobilization. Heavily p-doped silicon (Hp-silicon) was found to generate a significant increase in photocurrent at 875 $\mu A\ cm^{-2}$, as directly compared to only 0.35 $\mu A\ cm^{-2}$ of the same conditions on gold electrodes [139]. This result by LeBlanc et al. was attributed to the favorable valance band alignment of silicon to the P_{700} site, allowing for a unidirectional flow of electrons from silicon to P_{700}, with methyl viologen accepting electrons at F_B [139]. Coupling its relative affordability and abundance to other metals, this work has shown silicon to be a highly attractive material for use in PSI-biohybrid devices. The next strategy by Mershin et al. [33] takes advantage of an increased electrode area for PSI deposition (estimated to be about 50 times per μm of film thickness) offered by the added dimension of the nanocrystalline TiO_2 and ZnO nanowires. Along with the nanostructured electrode surface, designer peptide surfactants (similar to that of Kiley et al. [29]) were utilized for PSI stabilization to prevent protein denaturation and retain functionality after the drying process. These methods were used in conjunction with the novel Z813 electrolyte to achieve a photocurrent of 362 $\mu A\ cm^{-2}$, the second highest reported value and highest value by over 3 orders of magnitude if normalized to excitation intensity (4469 $\mu A\ cm^{-2}\ mW^{-1}$).

In our systematic breakdown of the PSI-generated photocurrents (Table 1), we have identified some key characteristics that have contributed in increasing this value over 4 orders of magnitude since the initial

Table 1
Component breakdown of biohybrid devices with PSI-generated photocurrent. PSI source came from either plant (green) or cyanobacteria (orange). Electron donors were sodium ascorbate (NaAs), 2,6-dichlorophenolindophenol (DCIP/DCPIP), reduced ferricyanide [$K_4Fe(CN)_6$], osmium [$Os(bpy)_2Cl_2$]/Os-polymer, Z813 electrolytes, and ruthenium hexamine (RuHex). Acceptors included naphthoquinone derivative molecular wire (NQC_{15}/$NQC_{15}EV$), methyl viologen (MV), oxidized ferricyanide [$K_3Fe(CN)_6$], composite Bis-aniline nanoparticle-ferredoxin (Bis-aniline-NP; Fd), and methylene blue. Mediator concentrations are also reported when possible, with * indicating that the concentration was not reported or composite mixture was used. Reported photocurrents [a] are shown in (μA cm^{-2}) with increasing values from a gradient of bright red (lowest—0.04) to bright green (highest—875). Excitation wavelength (nm) and intensity (mW cm^{-2}) are shown, with the latter going from dark gray (lowest—0.081) to yellow (highest—190). Photocurrent values normalized [b] to 1 mW cm^{-2} of excitation intensity are then shown from bright red (lowest—0.0056) (μA cm^{-2} * mW) to bright green (highest—4469.1). Unavailable data is indicated by (–).

Photocurrent Analysis									
PSI Source	Electrode Surface/ Immobilization	Redox Mediators			Photocurrent[a] (μA cm^{-2})	Ex. Intensity (mW cm^{-2})	Wave-length (nm)	Current Density[b] (μA cm^{-2} mW^{-1})	Ref.
		Donor	Acceptor	Concentrations					
T.e.	Au nanoparticles/(SAM)/MPS/PSI	NaAs / DCIP	-	250mM / 2.5mM	1.6	3.3	680	0.48	[153]
T.e.	NQC15S-Au NP on gold	NaAs / DCPIP	*NQC_{15}**	250mM / 2.5mM	-	3.3	680	0.007	[162]
Spinach	TPDA-SAM on nanoporous gold	NaAs / DCIP	-	5mM / 0.25mM	0.3	3.7	(red filter)	0.08	[144]
Spinach	Bare gold	NaAs / DCPIP	-	5mM / 0.25mM	-	-	-	0.1	[143]
6803	Au-PSI-Pt-PSI-Pt-PSI	NaAs / DCIP	-	20mM / 0.05mM	120	40	670	3	[150]
T.e.	NQC15EV on gold	NaAs / DCIP	*$NQC_{15}EV$**	250mM / 0.25mM	0.04	0.32	680	0.125	[146]
T.e.	MPS-SAM	DCPIP	MV	250mM / 0.25mM	0.9	1.8	680	0.5	[147]
Spinach	PS I – Based biohybrid cells	NaAs / DCIP	-	100mM / 5mM	2	29	-	0.138	[103]
Spinach	Cysteamine-SA /PSI multilayer	$K_4Fe(CN)_6$	$K_3Fe(CN)_6$	0.1mM / 0.1mM	7.9	95	(white light)	0.083	[148]
M.l.	Bis-aniline-NP-Pt-Fd-NP/PSI composite	NaAs / DCPIP	*Bis-aniline-NP; Fd**	40mM / 0.056mM	1.38	1.13	420	1.22	[164]
T.e.	Osmium complex modified polymer	*Os complexes**	MV	2mM	29	1.8	680	16.1	[78]
Spinach	PSI films/p-doped silicon	-	MV	0.2mM	875	190	633	4.6	[139]
T.e.	Nanocrystalline TiO2/ZnO-psaD/E-PSI	*Z813 Co(II)/ Co(III)**	-	-	362	0.081	(full sun)	4469.1	[33]
Spinach	PSI-graphene	(RuHex)	Methylene Blue	0.2mM / 20mM	0.55	98	633	0.0056	[81]
T.e.	Alkanethiol-SAMs (MHO,MHA)	$Os(bpy)_2Cl_2$	MV	0.0135mM / 0.25mM	0.075	1.4	676	0.054	[136]

studies done a decade ago. The works done on PSI-biohybrids also extend to literature (Table 2) that primarily focuses on the characterization and analysis of PSI immobilization strategies that do not include a value for photocurrent. By providing insight into PSI functionality and detailed characterization after immobilization, these studies should be looked at in conjunction with photocurrent studies to maximize the potential of PSI on nanostructured biohybrid devices for the generation of *green* electricity.

10. Concluding remarks and future opportunities

Despite a relatively small number of laboratories worldwide working on applied photosynthesis, the collective progress is remarkable. In a short span of <10 years, the performance of these PSI based devices has increased more than 10,000 fold. Moreover, this work has been accomplished with a fraction of the research support that other areas of bioenergy research have enjoyed for the past decade. For example, the Bioenergy Research Centers at Oak Ridge, Wisconsin, and Berkeley have received approximately $375 million from 2007 to 2012 and will receive $325 million from 2013 to 2018 [170,171]. British Petroleum (BP) has also donated $500 million to UC Berkeley to lead energy research consortium to establish the Energy Biosciences Institute (EBI) [172]. On the other hand, there are still many challenges in funding for PSI biohybrid-based research. The need to develop rapid and inexpensive methods to purify PSI still needs to be explored. To that end, the recent demonstration that non-agricultural plants, such as *Pueraria lobata* (Kudzu), can be utilized as a source for PSI [173] suggests the possibility that any locally grown plant, including noxious weeds, can be good source of PSI.

This technology can build directly on the highly advanced and regionally adaptive processes of modern agriculture. The ability to grow a green leafy crop such as spinach and harvest PSI particles that can be

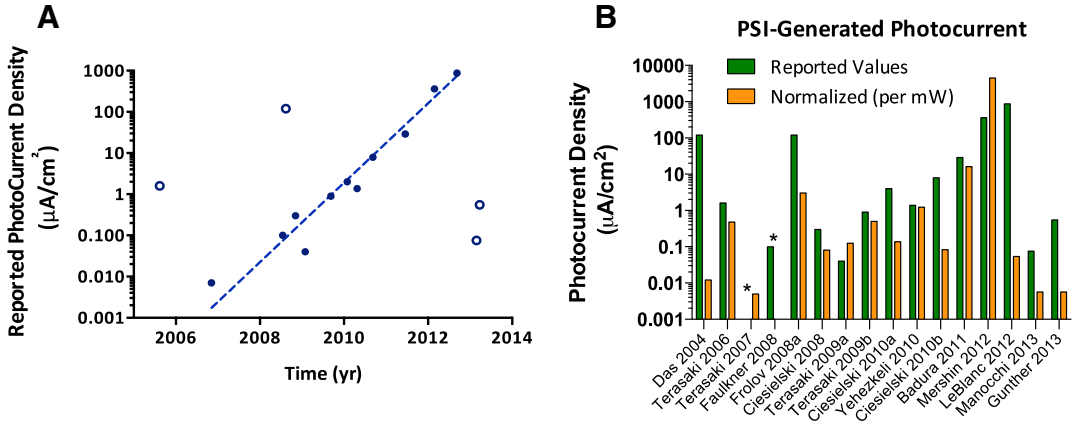

Fig. 8. Progress of PSI-generated photocurrent. (A) Photocurrent density extracted from PSI studies from 2005 to 2013. About a 10 fold increase in rate (μA cm^{-2}) is seen per year with the fitted trend line (open points excluded). (B) A comparison between the reported maximal current density and when normalized to 1 mW cm^{-2} of applied excitation intensity.*Unable to extrapolate both values due to lack of reported data.

Table 2
Various studies on strategies for PSI immobilization, characterization, and enhancement. PSI source, plant (green) and cyanobacteria (orange), electrode immobilization strategy, and PSI characterization/enhancement methods are described.

Characterization and Analysis of Immobilization Strategy			
PSI Source	**Electrode Surface/ Immobilization**	**Methods**	**Ref.**
Spinach	Au/alkanethiol-SAMs	Triton X-100, adsorbs to low-energy surfaces (hydrophobic SAM), and its PEG groups prevents protein adsorption.	[79]
6803	Au/SAM	PSI attachment by lumenal cysteins. Specific location not essential as long as on extramembranal loop.	[150]
Spinach	Au-coated-Ni-NTA glass	Designed peptide detergents, acetyl-AAAAAAK (A_6K), preserves PSI's native spectral properties/stabilizes PSI in the dry form for >3 wk.	[29]
Spinach	Hybrid Organosilicate Glass (Sol-gel)	Enables entrapment of PSI/offers a stabilizing environment for other biomolecules e.g. redox mediators. Matrix transparency is an advantage.	[156]
Spinach	PSI/HOC_6S/Au backfilled with $C_{22}SH$ or $C_{18}OC_{10}SH$	PSI on HOC6S/Au SAMs, followed by a backfilling of longer-chained methyl-terminated alkanethiols in the interprotein domains," mimics thylakoid".	[80]
6803	NP-PS I-NP	Showed that colloidal metal NPs (gold and silver) bound to PSI, acting as optical antennas, enable enhanced broad-band light absorption.	[161]
T.e.	hydroxyl-terminated alkanethiolate SAM/Au	Improved on PSI monolayer uniformity via an electric-field assisted deposition. Prevented PSI aggregates that normally formed with the more widely used gravity-driven deposition.	[31]
6803	PSI-CNT hybrids.	Three different strategies for on-chip functionalization of CNT-PSI hybrids were demonstrated (covalent bond, hydrogen bond, and electrostatic forces).	[155]
Spinach	PSI/aminoethanethiol-terephthaldialdehyde SAM	Developed mechanistic-kinetic model to investigate the various contributions to the photocurrent production / effects of adsorbed PSI orientation.	[145]
T.e.	PSI-PSII/Sol-Gel Glasses	Combinations of mediated coupling of PSII and/or PSI in solution or sol-gel encapsulated. Enables e^- flow from water photooxidized by PSII to PSI F_B.	[157]
T.e.	(Monomer/Trimer)PS I/alkanethiolate SAM/Au	Showed how temp., mono-/trimeric forms of PSI, and detergent used affects PSI adsorption, along with gravity driven versus an electric field assisted assembly.	[32]
M.l.	PQQ/PSI/(DNaAs/DCPIP)	Anodic/cathodic switchability of photocurrent via PQQ/CdS QDs/(TEOA) or PQQ/PSI/(DNaAs/DCPIP) under various photoelectrochemical configurations.	[149]
6803	PSI/Au	Photocurrent of an individual PSI via SNOM shows the preservation of its native biomolecular properties after being integrated into nanodevices.	[160]
6803	PSI/Mesoporous TiO2 Films	TiO_2 matrix's larger pore diameter allowed for a high concentration of PSI to be immobilized, allowing the complex to absorb higher light levels.	[152]
N/A	N/A	Computational model for dipole calculations, luminal surface hydropathicity and polarity characterization were used to predict improvements in surface-assembled monolayer design.	[35]

integrated into a device that may function for many weeks [130], months [10], or even years [103] suggests that the requisite agricultural investment (in terms of both energy, water, land and capital) may be highly amortized and possibly insignificant. These are issues that other competing bioenergy solutions, such as cellulosic ethanol and algal biodiesel, are still struggling to address and overcome [174–178].

The ability to "grow once and use many" is fundamentally different to other biomass based energy solutions, which are all single harvest based processes. We have calculated that a single acre of land in the Salinas valley can yield nearly 100,000 lbs of spinach leaves per year. Using current protocols of PSI isolation this one acre can yield ~6.8×10^{20} particles of PSI, which if applied as a uniform, single monolayer coating of a solar cell could yield 42 acres of solar cells assuming square packing. Although this technology is still emerging, the ability to couple the current advanced precision agricultural methods that exist with the rapidly evolving areas of biotechnology and nanotechnology does in fact suggest that one day we may in fact be able to *grow green electricity*.

Acknowledgements

BDB acknowledges support from TN-SCORE, a multi-disciplinary research program sponsored by NSF-EPSCoR (EPS-1004083) and support from the Gibson Family Foundation. KN and BDB acknowledge support from the UTK BCMB Department. KN was supported as an IGERT Fellow from the National Science Foundation IGERT program (DGE-0801470). BDB and KN also acknowledge support from the Directors Strategic Initiative, "Understanding Photosystem I as a Biomolecular Reactor for Energy Conversion" at the Army Research Laboratory, Adelphi, MD (ARL Contract #W911NF-11-2-0029). We would like to thank R. Carter, R. Simmerman, Dr. Chotewutmontri, and M. Vaughn for discussion and critically reading the manuscript. We would also like to thank M. Vaughn for assistance with the figures.

References

[1] N. Nelson, C.F. Yocum, Structure and function of photosystems I and II, Annu. Rev. Plant Biol. 57 (2006) 521–565.
[2] C.A. Kerfeld, D.W. Krogmann, Photosynthetic cytochromes c in cyanobacteria, algae, and plants, Annu. Rev. Plant Physiol. Plant Mol. Biol. 49 (1998) 397–425.
[3] N.V. Karapetyan, The dynamics of excitation energy in photosystem I of cyanobacteria: transfer in the antenna, capture by the reaction site, and dissipation, Biofizika 49 (2004) 212–226.
[4] N.V. Karapetyan, A.R. Holzwarth, M. Rogner, The photosystem I trimer of cyanobacteria: molecular organization, excitation dynamics and physiological significance, FEBS Lett. 460 (1999) 395–400.
[5] B. Ke, Primary electron-acceptor of photosystem I, Biochim. Biophys. Acta 301 (1973) 1–33.
[6] M. Medina, Structural and mechanistic aspects of flavoproteins: photosynthetic electron transfer from photosystem I to $NADP^+$, FEBS J. 276 (2009) 3942–3958.
[7] S. Santabarbara, P. Heathcote, M.C.W. Evans, Modelling of the electron transfer reactions in Photosystem I by electron tunnelling theory: the phylloquinones bound to the PsaA and the PsaB reaction centre subunits of PSI are almost isoenergetic to the iron–sulfur cluster Fx, Biochim. Biophys. Acta Bioenerg. 1708 (2005) 283–310.
[8] A.Y. Semenov, S.K. Chamorovsky, M.D. Mamedov, Electrogenic reactions in photosystem I complexes, Biofizika 49 (2004) 227–238.
[9] P. Setif, Ferredoxin and flavodoxin reduction by photosystem I, Biochim. Biophys. Acta Bioenerg. 1507 (2001) 161–179.
[10] I.J. Iwuchukwu, M. Vaughn, N. Myers, H. O'Neill, P. Frymier, B.D. Bruce, Self-organized photosynthetic nanoparticle for cell-free hydrogen production, Nat. Nanotechnol. 5 (2010) 73–79.
[11] I.J. Iwuchukwu, E. Iwuchukwu, R. Le, C. Paquet, R. Sawhney, B. Bruce, P. Frymier, Optimization of photosynthetic hydrogen yield from platinized photosystem I complexes using response surface methodology, Int. J. Hydrogen Energy 36 (2011) 11684–11692.
[12] A. Mershin, K. Matsumoto, L. Kaiser, D. Yu, M. Vaughn, M.K. Nazeeruddin, B.D. Bruce, M. Graetzel, S. Zhang, Self-assembled photosystem-I biophotovoltaics on nanostructured $TiO_2$and ZnO, Sci. Rep. 2 (2012) 234.
[13] D. Mukherjee, M. Vaughn, B. Khomami, B.D. Bruce, Modulation of cyanobacterial photosystem I deposition properties on alkanethiolate Au substrate by various experimental conditions, Colloids Surf. B Biointerfaces 88 (2011) 181–190.
[14] A. Amunts, N. Nelson, Plant photosystem I design in the light of evolution, Structure 17 (2009) 637–650.
[15] C.E. Lubner, M. Heinnickel, D.A. Bryant, J.H. Golbeck, Wiring photosystem I for electron transfer to a tethered redox dye, Energy Environ. Sci. 4 (2011) 2428–2434.
[16] L.M. Utschig, S.C. Silver, K.L. Mulfort, D.M. Tiede, Nature-driven photochemistry for catalytic solar hydrogen production: a photosystem I–transition metal catalyst hybrid, J. Am. Chem. Soc. 133 (2011) 16334–16337.
[17] Y. Mazor, I. Greenberg, H. Toporik, O. Beja, N. Nelson, The evolution of photosystem I in light of phage-encoded reaction centres, Philos. Trans. R. Soc. B 367 (2012) 3400–3405.
[18] G. Hauska, T. Schoedl, H. Remigy, G. Tsiotis, The reaction center of green sulfur bacteria, Biochim. Biophys. Acta Bioenerg. 1507 (2001) 260–277.

[19] U. Liebl, M. Mockensturmwilson, J.T. Trost, D.C. Brune, R.E. Blankenship, W. Vermaas, Single core polypeptide in the reaction-center of the photosynthetic bacterium *Heliobacillus mobilis* — structural implications and relations to other photosystems, Proc. Natl. Acad. Sci. U. S. A. 90 (1993) 7124–7128.

[20] A.W. Rutherford, M.C.W. Evans, Direct measurement of the redox potential of the primary and secondary quinone electron-acceptors in Rhodopseudomonas sphaeroides (wild-type) by electron-paramagnetic-res spectrometry, FEBS Lett. 110 (1980) 257–261.

[21] J.H.A. Nugent, Oxygenic photosynthesis — electron transfer in photosystem I and photosystem II, Eur. J. Biochem. 237 (1996) 519–531.

[22] C.E. Lubner, P. Knorzer, P.J.N. Silva, K.A. Vincent, T. Happe, D.A. Bryant, J.H. Golbeck, Wiring an [FeFe]-hydrogenase with photosystem I for light-induced hydrogen production, Biochemistry 49 (2010) 10264–10266.

[23] C.E. Lubner, R. Grimme, D.A. Bryant, J.H. Golbeck, Wiring photosystem I for direct solar hydrogen production, Biochemistry 49 (2010) 404–414.

[24] J.F. Millsaps, B.D. Bruce, J.W. Lee, E. Greenbaum, Nanoscale photosynthesis: photocatalytic production of hydrogen by platinized photosystem I reaction centers, Photochem. Photobiol. 73 (2001) 630–635.

[25] B.R. Evans, H.M. O'Neill, S.A. Hutchens, B.D. Bruce, E. Greenbaum, Enhanced photocatalytic hydrogen evolution by covalent attachment of plastocyanin to photosystem I, Nano Lett. 4 (2004) 1815–1819.

[26] N. Nelson, Plant photosystem I — the most efficient nano-photochemical machine, J. Nanosci. Nanotechnol. 9 (2009) 1709–1713.

[27] N. Nelson, Photosystems and global effects of oxygenic photosynthesis, Biochim. Biophys. Acta Bioenerg. 1807 (2011) 856–863.

[28] N. Nelson, Evolution of photosystem I and the control of global enthalpy in an oxidizing world, Photosynth. Res. 116 (2013) 145–151.

[29] P. Kiley, X.J. Zhao, M. Vaughn, M.A. Baldo, B.D. Bruce, S.G. Zhang, Self-assembling peptide detergents stabilize isolated photosystem I on a dry surface for an extended time, PLoS Biol. 3 (2005) 1180–1186.

[30] K. Matsumoto, M. Vaughn, B.D. Bruce, S. Koutsopoulos, S.G. Zhang, Designer peptide surfactants stabilize functional photosystem-I membrane complex in aqueous solution for extended time, J. Phys. Chem. B 113 (2009) 75–83.

[31] D. Mukherjee, M. May, M. Vaughn, B.D. Bruce, B. Khomami, Controlling the morphology of photosystem I assembly on thiol-activated Au substrates, Langmuir 26 (2010) 16048–16054.

[32] D. Mukherjee, M. Vaughn, B. Khomami, B.D. Bruce, Modulation of cyanobacterial photosystem I deposition properties on alkanethiolate Au substrate by various experimental conditions, Colloids Surf. B 88 (2011) 181–190.

[33] A. Mershin, K. Matsumoto, L. Kaiser, D.Y. Yu, M. Vaughn, M.K. Nazeeruddin, B.D. Bruce, M. Graetzel, S.G. Zhang, Self-assembled photosystem-I biophotovoltaics on nanostructured TiO_2 and ZnO, Sci. Rep. 2 (2012).

[34] D.R. Baker, A.K. Manocchi, S. Pendley, J.J. Sumner, M. Hurley, K. Xu, B.D. Bruce, C.A. Lundgren, Photosystem I based solar cell for on-site hydrogen production, Abstr. Pap. Am. Chem. Soc. 243 (2012).

[35] S.S. Pendley, M.M. Hurley, A. Mannochi, D. Baker, J.J. Sumner, C. Lundgren, B.D. Bruce, Re-engineering photosystem I as a photocatalytic hydrogen producing reactor, Abstr. Pap. Am. Chem. Soc. 243 (2012).

[36] A.K. Manocchi, D.R. Baker, J.J. Sumner, S.S. Pendley, M.M. Hurley, K. Xu, B.D. Bruce, C.A. Lundgren, Surface-assembled Photosystem I as a biomolecular reactor toward solar energy conversion, Abstr. Pap. Am. Chem. Soc. 244 (2012).

[37] A.K. Manocchi, D.R. Baker, S.S. Pendley, K. Nguyen, M.M. Hurley, B.D. Bruce, J.J. Sumner, C.A. Lundgren, Photocurrent generation from surface assembled photosystem I on alkanethiol modified electrodes, Langmuir 29 (2013) 2412–2419.

[38] K. Patel, M. Bigler, J. Hill, B. Morgan, B.D. Bruce, N. Phambu, Raman investigation of the interaction of photosystem I with highly ordered pyrolytic graphite, Abstr. Pap. Am. Chem. Soc. 245 (2013).

[39] A. Nakamura, T. Suzawa, Y. Kato, T. Watanabe, Species dependence of the redox potential of the primary electron donor P700 in photosystem I of oxygenic photosynthetic organisms revealed by spectroelectrochemistry, Plant Cell Physiol. 52 (2011) 815–823.

[40] T. Tomo, Y. Kato, T. Suzuki, S. Akimoto, T. Okubo, T. Noguchi, K. Hasegawa, T. Tsuchiya, K. Tanaka, M. Fukuya, N. Dohmae, T. Watanabe, M. Mimuro, Characterization of highly purified photosystem I complexes from the chlorophyll d-dominated cyanobacterium *Acaryochloris marina* MBIC 11017, J. Biol. Chem. 283 (2008) 18198–18209.

[41] M. Schenderlein, M. Cetin, J. Barber, A. Telfer, E. Schlodder, Spectroscopic studies of the chlorophyll d containing photosystem I from the cyanobacterium, *Acaryochloris marina*, Biochim. Biophys. Acta 1777 (2008) 1400–1408.

[42] R.E. Blankenship, D.M. Tiede, J. Barber, G.W. Brudvig, G. Fleming, M. Ghirardi, M.R. Gunner, W. Junge, D.M. Kramer, A. Melis, T.A. Moore, C.C. Moser, D.G. Nocera, A.J. Nozik, D.R. Ort, W.W. Parson, R.C. Prince, R.T. Sayre, Comparing photosynthetic and photovoltaic efficiencies and recognizing the potential for improvement, Science 332 (2011) 805–809.

[43] J. Deisenhofer, O. Epp, K. Miki, R. Huber, H. Michel, X-ray structure-analysis of a membrane–protein complex — electron-density map at 3a resolution and a model of the chromophores of the photosynthetic reaction center from *Rhodopseudomonas viridis*, J. Mol. Biol. 180 (1984) 385–398.

[44] J. Deisenhofer, O. Epp, K. Miki, R. Huber, H. Michel, Structure of the protein subunits in the photosynthetic reaction center of *Rhodopseudomonas viridis* at 3a resolution, Nature 318 (1985) 618–624.

[45] P. Jordan, P. Fromme, H.T. Witt, O. Klukas, W. Saenger, N. Krauss, Three-dimensional structure of cyanobacterial photosystem I at 2.5 Å resolution, Nature 411 (2001) 909–917.

[46] K.N. Ferreira, T.M. Iverson, K. Maghlaoui, J. Barber, S. Iwata, Architecture of the photosynthetic oxygen-evolving center, Science 303 (2004) 1831–1838.

[47] E. El-Mohsnawy, M.J. Kopczak, E. Schlodder, M. Nowaczyk, H.E. Meyer, B. Warscheid, N.V. Karapetyan, M. Rogner, Structure and function of intact photosystem 1 monomers from the cyanobacterium *Thermosynechococcus elongatus*, Biochemistry 49 (2010) 4740–4751.

[48] B. Bottcher, P. Graber, E.J. Boekema, The structure of Photosystem I from the thermophilic cyanobacterium *Synechococcus* sp. determined by electron microscopy of two-dimensional crystals, Biochim. Biophys. Acta 1100 (1992) 125–136.

[49] J. Kruip, P.R. Chitnis, B. Lagoutte, M. Rogner, E.J. Boekema, Structural organization of the major subunits in cyanobacterial photosystem 1. Localization of subunits PsaC, -D, -E, -F, and -J, J. Biol. Chem. 272 (1997) 17061–17069.

[50] D. Fotiadis, D.J. Muller, G. Tsiotis, L. Hasler, P. Tittmann, T. Mini, P. Jeno, H. Gross, A. Engel, Surface analysis of the photosystem I complex by electron and atomic force microscopy, J. Mol. Biol. 283 (1998) 83–94.

[51] D. Kaftan, V. Brumfeld, R. Nevo, A. Scherz, Z. Reich, From chloroplasts to photosystems: in situ scanning force microscopy on intact thylakoid membranes, EMBO J. 21 (2002) 6146–6153.

[52] H.N. Chapman, P. Fromme, A. Barty, T.A. White, R.A. Kirian, A. Aquila, M.S. Hunter, J. Schulz, D.P. DePonte, U. Weierstall, R.B. Doak, F.R.N.C. Maia, A.V. Martin, I. Schlichting, L. Lomb, N. Coppola, R.L. Shoeman, S.W. Epp, R. Hartmann, D. Rolles, A. Rudenko, L. Foucar, N. Kimmel, G. Weidenspointner, P. Holl, M.N. Liang, M. Barthelmess, C. Caleman, S. Boutet, M.J. Bogan, J. Krzywinski, C. Bostedt, S. Bajt, L. Gumprecht, B. Rudek, B. Erk, C. Schmidt, A. Homke, C. Reich, D. Pietschner, L. Struder, G. Hauser, H. Gorke, J. Ullrich, S. Herrmann, G. Schaller, F. Schopper, H. Soltau, K.U. Kuhnel, M. Messerschmidt, J.D. Bozek, S.P. Hau-Riege, M. Frank, C.Y. Hampton, R.G. Sierra, D. Starodub, G.J. Williams, J. Hajdu, N. Timneanu, M.M. Seibert, J. Andreasson, A. Rocker, O. Jonsson, M. Svenda, S. Stern, K. Nass, R. Andritschke, C.D. Schroter, F. Krasniqi, M. Bott, K.E. Schmidt, X.Y. Wang, I. Grotjohann, J.M. Holton, T.R.M. Barends, R. Neutze, S. Marchesini, R. Fromme, S. Schorb, D. Rupp, M. Adolph, T. Gorkhover, I. Andersson, H. Hirsemann, G. Potdevin, H. Graafsma, B. Nilsson, J.C.H. Spence, Femtosecond X-ray protein nanocrystallography, Nature 470 (2011) 73-U81.

[53] A. Ben-Shem, F. Frolow, N. Nelson, Crystal structure of plant photosystem I, Nature 426 (2003) 630–635.

[54] A. Amunts, O. Drory, N. Nelson, The structure of a plant photosystem I supercomplex at 3.4 Å resolution, Nature 447 (2007) 58–63.

[55] M. Beissinger, H. Sticht, M. Sutter, A. Ejchart, W. Haehnel, P. Rosch, Solution structure of cytochrome c_6 from the thermophilic cyanobacterium *Synechococcus elongatus*, EMBO J. 17 (1998) 27–36.

[56] H. Hatanaka, R. Tanimura, S. Katoh, F. Inagaki, Solution structure of ferredoxin from the thermophilic cyanobacterium *Synechococcus elongatus* and its thermostability, J. Mol. Biol. 268 (1997) 922–933.

[57] D.M. Hoover, C.L. Drennan, A.L. Metzger, C. Osborne, C.H. Weber, K.A. Pattridge, M.L. Ludwig, Comparisons of wild-type and mutant flavodoxins from *Anacystis nidulans*. Structural determinants of the redox potentials, J. Mol. Biol. 294 (1999) 725–743.

[58] M.L. Antonkine, G.H. Liu, D. Bentrop, D.A. Bryant, I. Bertini, C. Luchinat, J.H. Golbeck, D. Stehlik, Solution structure of the unbound, oxidized photosystem I subunit PsaC, containing [4Fe–4S] clusters F-A and F-B: a conformational change occurs upon binding to photosystem I, J. Biol. Inorg. Chem. 7 (2002) 461–472.

[59] Z.C. Xia, R.W. Broadhurst, E.D. Laue, D.A. Bryant, J.H. Golbeck, D.S. Bendall, Structure and properties in solution of PsaD, an extrinsic polypeptide of photosystem I, Eur. J. Biochem. 255 (1998) 309–316.

[60] C.J. Falzone, Y.H. Kao, J.D. Zhao, K.L. Maclaughlin, D.A. Bryant, J.T.J. Lecomte, ^{1}H and ^{15}N NMR assignments of PsaE, a photosystem I subunit from the cyanobacterium *Synechococcus* sp. strain PCC-7002, Biochemistry 33 (1994) 6043–6051.

[61] I. Marton, A. Zuker, E. Shklarman, V. Zeevi, A. Tovkach, S. Roffe, M. Ovadis, T. Tzfira, A. Vainstein, Nontransgenic genome modification in plant cells, Plant Physiol. 154 (2010) 1079–1087.

[62] T. Tzfira, D. Weinthal, I. Marton, V. Zeevi, A. Zuker, A. Vainstein, Genome modifications in plant cells by custom-made restriction enzymes, Plant Biotechnol. J. 10 (2012) 373–389.

[63] W.S. Liu, J.S. Yuan, C.N. Stewart, Advanced genetic tools for plant biotechnology, Nat. Rev. Genet. 14 (2013) 781–793.

[64] D.J. Caruana, S. Howorka, Biosensors and biofuel cells with engineered proteins, Mol. Biosyst. 6 (2010) 1548–1556.

[65] S.A. Ansari, Q. Husain, Potential applications of enzymes immobilized on/in nano materials: a review, Biotechnol. Adv. 30 (2012) 512–523.

[66] C. You, Y.H.P. Zhang, Cell-free biosystems for biomanufacturing, Adv. Biochem. Eng. Biotechnol. 131 (2013) 89–119.

[67] J.H. Golbeck, A comparative analysis of the spin state distribution of in vitro and in vivo mutants of PsaC — a biochemical argument for the sequence of electron transfer in photosystem I as F-X → F-A → F-B → ferredoxin/flavodoxin, Photosynth. Res. 61 (1999) 107–144.

[68] S. Izawa, Acceptors and donors and chloroplast electron transport, Methods Enzymol. 69 (1980) 413–434.

[69] R. Das, P.J. Kiley, M. Segal, J. Norville, A.A. Yu, L.Y. Wang, S.A. Trammell, L.E. Reddick, R. Kumar, F. Stellacci, N. Lebedev, J. Schnur, B.D. Bruce, S.G. Zhang, M. Baldo, Integration of photosynthetic protein molecular complexes in solid-state electronic devices, Nano Lett. 4 (2004) 1079–1083.

[70] J.D. Zhao, P.V. Warren, N. Li, D.A. Bryant, J.H. Golbeck, Reconstitution of electron transport in photosystem I with PsaC and PsaD proteins expressed in *Escherichia coli*, FEBS Lett. 276 (1990) 175–180.

[71] L. Minai, Y. Cohen, P.R. Chitnis, R. Nechushtai, The precursor of PsaD assembles into the photosystem I complex in two steps, Proc. Natl. Acad. Sci. U. S. A. 93 (1996) 6338–6342.

[72] L. Minai, A. Fish, M. Darash-Yahana, L. Verchovsky, R. Nechushtai, The assembly of the PsaD subunit into the membranal photosystem I complex occurs via an exchange mechanism, Biochemistry 40 (2001) 12754–12760.

[73] A. Lushy, L. Verchovsky, R. Nechushtai, The stable assembly of newly synthesized PsaE into the photosystem I complex occurring via the exchange mechanism is facilitated by electrostatic interactions, Biochemistry 41 (2002) 11192–11199.

[74] E.M. Aro, I. Virgin, B. Andersson, Photoinhibition of photosystem II. Inactivation, protein damage and turnover, Biochim. Biophys. Acta 1143 (1993) 113–134.

[75] J. Barber, B. Andersson, Too much of a good thing: light can be bad for photosynthesis, Trends Biochem. Sci. 17 (1992) 61–66.

[76] M. Hervas, M.A. De la Rosa, G. Tollin, A comparative laser-flash absorption spectroscopy study of algal plastocyanin and cytochrome c_{552} photooxidation by photosystem I particles from spinach, Eur. J. Biochem. 203 (1992) 115–120.

[77] D.R. Ort, S. Izawa, Studies on the energy-coupling sites of photophosphorylation: V. Phosphorylation efficiencies (P/e_2) associated with aerobic photooxidation of artificial electron donors, Plant Physiol. 53 (1974) 370–376.

[78] A. Badura, D. Guschin, T. Kothe, M.J. Kopczak, W. Schuhmann, M. Rogner, Photocurrent generation by photosystem 1 integrated in crosslinked redox hydrogels, Energy Environ. Sci. 4 (2011) 2435–2440.

[79] B.S. Ko, B. Babcock, G.K. Jennings, S.G. Tilden, R.R. Peterson, D. Cliffel, E. Greenbaum, Effect of surface composition on the adsorption of photosystem I onto alkanethiolate self-assembled monolayers on gold, Langmuir 20 (2004) 4033–4038.

[80] H.A. Kincaid, T. Niedringhaus, M. Ciobanu, D.E. Cliffel, G.K. Jennings, Entrapment of photosystem I within self-assembled films, Langmuir 22 (2006) 8114–8120.

[81] D. Gunther, G. LeBlanc, D. Prasai, J.R. Zhang, D.E. Cliffel, K.I. Bolotin, G.K. Jennings, Photosystem I on graphene as a highly transparent, photoactive electrode, Langmuir 29 (2013) 4177–4180.

[82] R.C. Ford, A. Holzenburg, Investigation of the structure of trimeric and monomeric photosystem I reaction centre complexes, EMBO J. 7 (1988) 2287–2293.

[83] J. Kruip, D. Bald, E. Boekema, M. Rögner, Evidence for the existence of trimeric and monomeric Photosystem I complexes in thylakoid membranes from cyanobacteria, Photosynth. Res. 40 (1994) 279–286.

[84] O. Almog, G. Shoham, D. Michaeli, R. Nechushtai, Monomeric and trimeric forms of photosystem I reaction center of *Mastigocladus laminosus*: crystallization and preliminary characterization, Proc. Natl. Acad. Sci. U. S. A. 88 (1991) 5312–5316.

[85] L. Garczarek, G.W.M. van der Staay, J.C. Thomas, F. Partensky, Isolation and characterization of Photosystem I from two strains of the marine oxychlorobacterium *Prochlorococcus*, Photosynth. Res. 56 (1998) 131–141.

[86] T.S. Bibby, I. Mary, J. Nield, F. Partensky, J. Barber, Low-light-adapted *Prochlorococcus* species possess specific antennae for each photosystem, Nature 424 (2003) 1051–1054.

[87] D. Mangels, J. Kruip, S. Berry, M. Rogner, E.J. Boekema, F. Koenig, Photosystem I from the unusual cyanobacterium *Gloeobacter violaceus*, Photosynth. Res. 72 (2002) 307–319.

[88] G. Tsiotis, W. Haase, A. Engel, H. Michel, Isolation and structural characterization of trimeric cyanobacterial photosystem I complex with the help of recombinant antibody fragments, Eur. J. Biochem. 231 (1995) 823–830.

[89] E.J. Boekema, A. Hifney, A.E. Yakushevska, M. Piotrowski, W. Keegstra, S. Berry, K.P. Michel, E.K. Pistorius, J. Kruip, A giant chlorophyll–protein complex induced by iron deficiency in cyanobacteria, Nature 412 (2001) 745–748.

[90] M. Brecht, M. Hussels, E. Schlodder, N.V. Karapetyan, Red antenna states of Photosystem I trimers from *Arthrospira platensis* revealed by single-molecule spectroscopy, Biochim. Biophys. Acta Bioenerg. 1817 (2012) 445–452.

[91] D.L. Tucker, L.A. Sherman, Analysis of chlorophyll–protein complexes from the cyanobacterium *Cyanothece* sp. ATCC 51142 by non-denaturing gel electrophoresis, Biochim. Biophys. Acta Biomembr. 1468 (2000) 150–160.

[92] J. Kruip, E.J. Boekema, D. Bald, A.F. Boonstra, M. Rogner, Isolation and structural characterization of monomeric and trimeric photosystem I complexes (P700·Fa/Fb and P700·Fx) from the cyanobacterium *Synechocystis* Pcc-6803, J. Biol. Chem. 268 (1993) 23353–23360.

[93] P. Jordan, P. Fromme, H.T. Witt, O. Klukas, W. Saenger, N. Krauss, Three-dimensional structure of cyanobacterial photosystem I at 2.5 Å resolution, Nature 411 (2001) 909–917.

[94] V.P. Chitnis, Q. Xu, L. Yu, J.H. Golbeck, H. Nakamoto, D.L. Xie, P.R. Chitnis, Targeted inactivation of the gene psaL encoding a subunit of photosystem I of the cyanobacterium *Synechocystis* sp. PCC 6803, J. Biol. Chem. 268 (1993) 11678–11684.

[95] V.P. Chitnis, P.R. Chitnis, PsaL subunit is required for the formation of photosystem I trimers in the cyanobacterium *Synechocystis* sp. PCC 6803, FEBS Lett. 336 (1993) 330–334.

[96] W.M. Schluchter, G.H. Shen, J.D. Zhao, D.A. Bryant, Characterization of psaI and psaL mutants of *Synechococcus* sp. strain PCC 7002: a new model for state transitions in cyanobacteria, Photochem. Photobiol. 64 (1996) 53–66.

[97] C.L. Aspinwall, M. Sarcina, C.W. Mullineaux, Phycobilisome mobility in the cyanobacterium *Synechococcus* sp. PCC7942 is influenced by the trimerisation of Photosystem I, Photosynth. Res. 79 (2004) 179–187.

[98] A. Ben-Shem, F. Frolow, N. Nelson, Evolution of photosystem I — from symmetry through pseudosymmetry to asymmetry, FEBS Lett. 564 (2004) 274–280.

[99] A. Amunts, N. Nelson, Functional organization of a plant Photosystem I: evolution of a highly efficient photochemical machine, Plant Physiol. Biochem. 46 (2008) 228–237.

[100] N. Nelson, A. Ben-Shem, The structure of photosystem I and evolution of photosynthesis, Bioessays 27 (2005) 914–922.

[101] Y. Nakamura, T. Kaneko, S. Sato, M. Ikeuchi, H. Katoh, S. Sasamoto, A. Watanabe, M. Iriguchi, K. Kawashima, T. Kimura, Y. Kishida, C. Kiyokawa, M. Kohara, M. Matsumoto, A. Matsuno, N. Nakazaki, S. Shimpo, M. Sugimoto, C. Takeuchi, M. Yamada, S. Tabata, Complete genome structure of the thermophilic cyanobacterium *Thermosynechococcus elongatus* BP-1, DNA Res. 9 (2002) 123–130.

[102] P. Kiley, X. Zhao, M. Vaughn, M.A. Baldo, B.D. Bruce, S. Zhang, Self-assembling peptide detergents stabilize isolated photosystem I on a dry surface for an extended time, PLoS Biol. 3 (2005) e230.

[103] P.N. Ciesielski, F.M. Hijazi, A.M. Scott, C.J. Faulkner, L. Beard, K. Emmett, S.J. Rosenthal, D. Cliffel, G.K. Jennings, Photosystem I — based biohybrid photoelectrochemical cells, Bioresour. Technol. 101 (2010) 3047–3053.

[104] W.F.J. Vermaas, Molecular-genetic approaches to study photosynthetic and respiratory electron-transport in thylakoids from cyanobacteria, Biochim. Biophys. Acta Bioenerg. 1187 (1994) 181–186.

[105] P.R. Chitnis, Q. Xu, V.P. Chitnis, R. Nechushtai, Function and organization of Photosystem I polypeptides, Photosynth. Res. 44 (1995) 23–40.

[106] H.B. Pakrasi, Genetic analysis of the form and function of photosystem I and photosystem II, Annu. Rev. Genet. 29 (1995) 755–776.

[107] H. Masukawa, M. Kitashima, K. Inoue, H. Sakurai, R.P. Hausinger, Genetic engineering of cyanobacteria to enhance biohydrogen production from sunlight and water, Ambio 41 (2012) 169–173.

[108] A. Tiwari, A. Pandey, Cyanobacterial hydrogen production — a step towards clean environment, Int. J. Hydrogen Energy 37 (2012) 139–150.

[109] K. Srirangan, M.E. Pyne, C.P. Chou, Biochemical and genetic engineering strategies to enhance hydrogen production in photosynthetic algae and cyanobacteria, Bioresour. Technol. 102 (2011) 8589–8604.

[110] T. Heidorn, D. Camsund, H.H. Huang, P. Lindberg, P. Oliveira, K. Stensjo, P. Lindblad, Synthetic biology in cyanobacteria: engineering and analyzing novel functions, Methods Enzymol. 497 (2011) 539–579.

[111] J.W.K. Oliver, I.M.P. Machado, H. Yoneda, S. Atsumi, Cyanobacterial conversion of carbon dioxide to 2,3-butanediol, Proc. Natl. Acad. Sci. U. S. A. 110 (2013) 1249–1254.

[112] J.C.F. Ortiz-Marquez, M. Do Nascimento, J.P. Zehr, L. Curatti, Genetic engineering of multispecies microbial cell factories as an alternative for bioenergy production, Trends Biotechnol. 31 (2013) 521–529.

[113] P.H. Chen, H.L. Liu, Y.J. Chen, H. Cheng, W.L. Lin, C.H. Yeh, C.H. Chang, Enhancing CO_2 bio-mitigation by genetic engineering of cyanobacteria, Energy Environ. Sci. 5 (2012) 8318–8327.

[114] A. Parmar, N.K. Singh, A. Pandey, E. Gnansounou, D. Madamwar, Cyanobacteria and microalgae: a positive prospect for biofuels, Bioresour. Technol. 102 (2011) 10163–10172.

[115] P. Lindberg, S. Park, A. Melis, Engineering a platform for photosynthetic isoprene production in cyanobacteria, using *Synechocystis* as the model organism, Metab. Eng. 12 (2010) 70–79.

[116] R. Radakovits, R.E. Jinkerson, A. Darzins, M.C. Posewitz, Genetic engineering of algae for enhanced biofuel production, Eukaryot. Cell 9 (2010) 486–501.

[117] H. Li, J.C. Liao, Engineering a cyanobacterium as the catalyst for the photosynthetic conversion of CO_2 to 1,2-propanediol, Microb. Cell Fact. 12 (2013).

[118] O. Pulz, W. Gross, Valuable products from biotechnology of microalgae, Appl. Microbiol. Biotechnol. 65 (2004) 635–648.

[119] S. Singh, B.N. Kate, U.C. Banerjee, Bioactive compounds from cyanobacteria and microalgae: an overview, Crit. Rev. Biotechnol. 25 (2005) 73–95.

[120] B. Wang, S. Pugh, D.R. Nielsen, W.W. Zhang, D.R. Meldrum, Engineering cyanobacteria for photosynthetic production of 3-hydroxybutyrate directly from CO_2, Metab. Eng. 16 (2013) 68–77.

[121] N.F. Tsinoremas, A.K. Kutach, C.A. Strayer, S.S. Golden, Efficient gene-transfer in *Synechococcus* sp. strains PCC-7942 and PCC-6301 by interspecies conjugation and chromosomal recombination, J. Bacteriol. 176 (1994) 6764–6768.

[122] U. Muhlenhoff, F. Chauvat, Gene transfer and manipulation in the thermophilic cyanobacterium synechococcus elongatus, Mol. Gen. Genet. 252 (1996) 93–100.

[123] W. Vermaas, Molecular genetics of the cyanobacterium *Synechocystis* sp. PCC 6803: principles and possible biotechnology applications, J. Appl. Phycol. 8 (1996) 263–273.

[124] F. Sommer, F. Drepper, M. Hippler, The luminal helix I of PsaB is essential for recognition of plastocyanin or cytochrome c_6 and fast electron transfer to photosystem I in *Chlamydomonas reinhardtii*, J. Biol. Chem. 277 (2002) 6573–6581.

[125] W. Xu, Y.C. Wang, E. Taylor, A. Laujac, L.Y. Gao, S. Savikhin, P.R. Chitnis, Mutational analysis of photosystem I of *Synechocystis* sp. PCC 6803: the role of four conserved aromatic residues in the j-helix of PsaB, PLoS One 6 (2011).

[126] Y. Takahashi, M. Goldschmidtclermont, S.Y. Soen, L.G. Franzen, J.D. Rochaix, Directed chloroplast transformation in *Chlamydomonas reinhardtii* — insertional inactivation of the Psac gene encoding the iron sulfur protein destabilizes photosystem I, EMBO J. 10 (1991) 2033–2040.

[127] R.M. Mannan, W.Z. He, S.U. Metzger, J. Whitmarsh, R. Malkin, H.B. Pakrasi, Active photosynthesis in cyanobacterial mutants with directed modifications in the ligands for two iron–sulfur clusters in the PsaC protein of photosystem I, EMBO J. 15 (1996) 1826–1833.

[128] J.P. Yu, L.B. Smart, Y.S. Jung, J. Golbeck, L. Mcintosh, Absence of PsaC subunit allows assembly of photosystem I core but prevents the binding of PsaD and PsaE in *Synechocystis* sp. PCC6803, Plant Mol. Biol. 29 (1995) 331–342.

[129] F. Rousseau, P. Setif, B. Lagoutte, Evidence for the involvement of Psi-E subunit in the reduction of ferredoxin by photosystem I, EMBO J. 12 (1993) 1755–1765.

[130] J. Zhao, W.B. Snyder, U. Muhlenhoff, E. Rhiel, P.V. Warren, J.H. Golbeck, D.A. Bryant, Cloning and characterization of the PsaE gene of the cyanobacterium *Synechococcus* sp. PCC 7002 — characterization of a PsaE mutant and overproduction of the protein in *Escherichia coli*, Mol. Microbiol. 9 (1993) 183–194.

[131] P.R. Chitnis, D. Purvis, N. Nelson, Molecular cloning and targeted mutagenesis of the gene psaF encoding subunit III of photosystem I from the cyanobacterium *Synechocystis* sp. PCC 6803, J. Biol. Chem. 266 (1991) 20146–20151.

[132] H. Kubota, I. Sakurai, K. Katayama, N. Mizusawa, S. Ohashi, M. Kobayashi, P.P. Zhang, E.M. Aro, H. Wada, Purification and characterization of photosystem I complex from *Synechocystis* sp. PCC 6803 by expressing histidine-tagged subunits, Biochim. Biophys. Acta Bioenerg. 1797 (2010) 98–105.
[133] H. Nakamoto, Targeted inactivation of the gene psaI encoding a subunit of photosystem I of the cyanobacterium *Synechocystis* sp. PCC 6803, Plant Cell Physiol. 36 (1995) 1579–1587.
[134] Q. Xu, W.R. Odom, J.A. Guikema, V.P. Chitnis, P.R. Chitnis, Targeted deletion of psaJ from the cyanobacterium *Synechocystis* sp. PCC-6803 indicates structural interactions between the PsaJ and PsaF subunits of photosystem I, Plant Mol. Biol. 26 (1994) 291–302.
[135] Q.A. Xu, L.A. Yu, V.P. Chitnis, P.R. Chitnis, Function and organization of photosystem I in a cyanobacterial mutant strain that lacks PsaF and PsaJ subunits, J. Biol. Chem. 269 (1994) 3205–3211.
[136] S. Naithani, J.M. Hou, P.R. Chitnis, Targeted inactivation of the psaK1, psaK2 and psaM genes encoding subunits of Photosystem I in the cyanobacterium *Synechocystis* sp. PCC 6803, Photosynth. Res. 63 (2000) 225–236.
[137] R.V. Duran, M. Hervas, B. De la Cerda, M.A. De la Rosa, J.A. Navarro, A laser flash-induced kinetic analysis of in vivo photosystem I reduction by site-directed mutants of plastocyanin and cytochrome c_6 in *Synechocystis* sp. PCC 6803, Biochemistry 45 (2006) 1054–1060.
[138] P. Setif, N. Fischer, B. Lagoutte, H. Bottin, J.D. Rochaix, The ferredoxin docking site of photosystem I, Biochim. Biophys. Acta Bioenerg. 1555 (2002) 204–209.
[139] G. LeBlanc, G. Chen, E.A. Gizzie, G.K. Jennings, D.E. Cliffel, Enhanced photocurrents of photosystem I films on p-doped silicon, Adv. Mater. 24 (2012) 5959–5962.
[140] G. LeBlanc, G. Chen, G.K. Jennings, D.E. Cliffel, Photoreduction of catalytic platinum particles using immobilized multilayers of photosystem I, Langmuir 28 (2012) 7952–7956.
[141] I. Lee, J.W. Lee, E. Greenbaum, Biomolecular electronics: vectorial arrays of photosynthetic reaction centers, Phys. Rev. Lett. 79 (1997) 3294–3297.
[142] M. Ciobanu, H.A. Kincaid, V. Lo, A.D. Dukes, G.K. Jennings, D.E. Cliffel, Electrochemistry and photoelectrochemistry of photosystem I adsorbed on hydroxyl-terminated monolayers, J. Electroanal. Chem. 599 (2007) 72–78.
[143] C.J. Faulkner, S. Lees, P.N. Ciesielski, D.E. Cliffel, G.K. Jennings, Rapid assembly of photosystem I monolayers on gold electrodes, Langmuir 24 (2008) 8409–8412.
[144] P.N. Ciesielski, A.M. Scott, C.J. Faulkner, B.J. Berron, D.E. Cliffel, G.K. Jennings, Functionalized nanoporous gold leaf electrode films for the immobilization of photosystem I, ACS Nano 2 (2008) 2465–2472.
[145] P.N. Ciesielski, D.E. Cliffel, G.K. Jennings, Kinetic model of the photocatalytic effect of a photosystem I monolayer on a planar electrode surface, J. Phys. Chem. A 115 (2011) 3326–3334.
[146] N. Terasaki, N. Yamamoto, T. Hiraga, Y. Yamanoi, T. Yonezawa, H. Nishihara, T. Ohmori, M. Sakai, M. Fujii, A. Tohri, M. Iwai, Y. Inoue, S. Yoneyama, M. Minakata, I. Enami, Plugging a molecular wire into photosystem I: reconstitution of the photoelectric conversion system on a gold electrode, Angew. Chem. Int. Ed. 48 (2009) 1585–1587.
[147] N. Terasaki, N. Yamamoto, M. Hattori, N. Tanigaki, T. Hiraga, K. Ito, M. Konno, M. Iwai, Y. Inoue, S. Uno, K. Nakazato, Photosensor based on an FET utilizing a biocomponent of photosystem I for use in imaging devices, Langmuir 25 (2009) 11969–11974.
[148] P.N. Ciesielski, C.J. Faulkner, M.T. Irwin, J.M. Gregory, N.H. Tolk, D.E. Cliffel, G.K. Jennings, Enhanced photocurrent production by photosystem I multilayer assemblies, Adv. Funct. Mater. 20 (2010) 4048–4054.
[149] A. Efrati, O. Yehezkeli, R. Tel-Vered, D. Michaeli, R. Nechushtai, I. Willner, Electrochemical switching of photoelectrochemical processes at CdS QDs and photosystem I-modified electrodes, ACS Nano 6 (2012) 9258–9266.
[150] L. Frolov, Y. Rosenwaks, C. Carmeli, I. Carmeli, Fabrication of a photoelectronic device by direct chemical binding of the photosynthetic reaction center protein to metal surfaces, Adv. Mater. 17 (2005) 2434(−+).
[151] L. Frolov, Y. Rosenwaks, S. Richter, C. Carmeli, I. Carmeli, Photoelectric junctions between GaAs and photosynthetic reaction center protein, J. Phys. Chem. C 112 (2008) 13426–13430.
[152] V.V. Nikandrov, Y.V. Borisova, E.A. Bocharov, M.A. Usachev, G.V. Nizova, V.A. Nadtochenko, E.P. Lukashev, B.V. Trubitsin, A.N. Tikhonov, V.N. Kurashov, M.D. Mamedov, A.Y. Semenov, Photochemical properties of photosystem 1 immobilized in a mesoporous semiconductor matrix, High Energy Chem. 46 (2012) 200–205.
[153] N. Terasaki, N. Yamamoto, T. Hiraga, I. Sato, Y. Inoue, S. Yamada, Fabrication of novel photosystem I–gold nanoparticle hybrids and their photocurrent enhancement, Thin Solid Films 499 (2006) 153–156.
[154] I. Carmeli, L. Frolov, C. Carmeli, S. Richter, Photovoltaic activity of photosystem I-based self-assembled monolayer, J. Am. Chem. Soc. 129 (2007) 12352(−+).
[155] S.M. Kaniber, M. Brandstetter, F.C. Simmel, I. Carmeli, A.W. Holleitner, On-chip functionalization of carbon nanotubes with photosystem I, J. Am. Chem. Soc. 132 (2010) 2872(−+).
[156] H. O'neill, E. Greenbaum, Spectroscopy and photochemistry of spinach photosystem I entrapped and stabilized in a hybrid organosilicate glass, Chem. Mater. 17 (2005) 2654–2661.
[157] F. Kopnov, I. Cohen-Ofri, D. Noy, Electron transport between photosystem II and photosystem I encapsulated in sol–gel glasses, Angew. Chem. Int. Ed. 50 (2011) 12347–12350.
[158] H. Toporik, I. Carmeli, I. Volotsenko, M. Molotskii, Y. Rosenwaks, C. Carmeli, N. Nelson, Large photovoltages generated by plant photosystem I crystals, Adv. Mater. 24 (2012) 2988–2991.
[159] O. Yehezkeli, R. Tel-Vered, D. Michaeli, R. Nechushtai, I. Willner, Photosystem I (PSI)/photosystem II (PSII)-based photo-bioelectrochemical cells revealing directional generation of photocurrents, Small 9 (2013) 2970–2978.
[160] D. Gerster, J. Reichert, H. Bi, J.V. Barth, S.M. Kaniber, A.W. Holleitner, I. Visoly-Fisher, S. Sergani, I. Carmeli, Photocurrent of a single photosynthetic protein, Nat. Nanotechnol. 7 (2012) 673–676.
[161] I. Carmeli, I. Lieberman, L. Kraversky, Z.Y. Fan, A.O. Govorov, G. Markovich, S. Richter, Broad band enhancement of light absorption in photosystem I by metal nanoparticle antennas, Nano Lett. 10 (2010) 2069–2074.
[162] N. Terasaki, N. Yamamoto, K. Tamada, M. Hattori, T. Hiraga, A. Tohri, I. Sato, M. Iwai, M. Iwai, S. Taguchi, I. Enami, Y. Inoue, Y. Yamanoi, T. Yonezawa, K. Mizuno, M. Murata, H. Nishihara, S. Yoneyama, M. Minakata, T. Ohmori, M. Sakai, M. Fujii, Bio-photo sensor: cyanobacterial photosystem I coupled with transistor via molecular wire, Biochim. Biophys. Acta Bioenerg. 1767 (2007) 653–659.
[163] L. Frolov, O. Wilner, C. Carmeli, I. Carmeli, Fabrication of oriented multilayers of photosystem I proteins on solid surfaces by auto-metallization, Adv. Mater. 20 (2008) 263(−+).
[164] O. Yehezkeli, O.I. Wilner, R. Tel-Vered, D. Roizman-Sade, R. Nechushtai, I. Willner, Generation of photocurrents by bis-aniline-cross-linked Pt nanoparticle/photosystem I composites on electrodes, J. Phys. Chem. B 114 (2010) 14383–14388.
[165] M. Miyachi, Y. Yamanoi, T. Yonezawa, H. Nishihara, M. Iwai, M. Konno, M. Iwai, Y. Inoue, Surface immobilization of PSI using vitamin K1-like molecular wires for fabrication of a bio-photoelectrode, J. Nanosci. Nanotechnol. 9 (2009) 1722–1726.
[166] M. Miyachi, Y. Yamanoi, Y. Shibata, H. Matsumoto, K. Nakazato, M. Konno, K. Ito, Y. Inoue, H. Nishihara, A photosensing system composed of photosystem I, molecular wire, gold nanoparticle, and double surfactants in water, Chem. Commun. (Camb.) 46 (2010) 2557–2559.
[167] J.W. Arblaster, Densities of osmium and iridium: recalculations based upon a review of the latest crystallographic data, Platinum Met. Rev. 33 (1989) 14–16.
[168] K.H. Wedepohl, The composition of the continental crust, Geochim. Cosmochim. Acta 59 (1995) 1217–1232.
[169] H. Nusbaumer, S.M. Zakeeruddin, J.E. Moser, M. Gratzel, An alternative efficient redox couple for the dye-sensitized solar cell system, Chem. Eur. J. 9 (2003) 3756–3763.
[170] Bioenergy Research Centers — Past Solicitations2007.
[171] DOE Bioenergy Research Centers2013.
[172] R. Sanders, BP Selects UC Berkeley to Lead $500 Million Energy Research Consortium with Partners, Lawrence Berkeley National Lab, University of Illinois, 2007.
[173] D. Gunther, *Pueraria lobata* (Kudzu) photosystem I improves the photoelectrochemical performance of silicon, Ind. Biotechnol. 9 (2013) 37–41.
[174] H.C.J. Godfray, J.R. Beddington, I.R. Crute, L. Haddad, D. Lawrence, J.F. Muir, J. Pretty, S. Robinson, S.M. Thomas, C. Toulmin, Food security: the challenge of feeding 9 billion people, Science 327 (2010) 812–818.
[175] K. Johansson, K. Liljequist, L. Ohlander, K. Aleklett, Agriculture as provider of both food and fuel, Ambio 39 (2010) 91–99.
[176] A. Singh, P.S. Nigam, J.D. Murphy, Renewable fuels from algae: an answer to debatable land based fuels, Bioresour. Technol. 102 (2011) 10–16.
[177] B.D. Solomon, Biofuels and sustainability, Ann. N. Y. Acad. Sci. 1185 (2010) 119–134.
[178] P.R.D. Williams, D. Inman, A. Aden, G.A. Heath, Environmental and sustainability factors associated with next-generation biofuels in the US: what do we really know? Environ. Sci. Technol. 43 (2009) 4763–4775.